Power Line Communication Channel Models for Home Area Networks

by

Xinyu Fang
B.Sc., Beijing University of Technology, 2011

A Thesis Submitted in Partial Fulfillment of the
Requirements for the Degree of

MASTER OF APPLIED SCIENCE

in the Department of Electrical and Computer Engineering

Power Line Communication Channel Models for Home Area Networks

by

Xinyu Fang
B.Sc., Beijing University of Technology, 2011

Supervisory Committee

Dr. T. Aaron Gulliver, Supervisor
(Department of Electrical and Computer Engineering)

Dr. Wu-Sheng Lu, Committee Member
(Department of Electrical and Computer Engineering)

Supervisory Committee

Dr. T. Aaron Gulliver, Supervisor
(Department of Electrical and Computer Engineering)

Dr. Wu-Sheng Lu, Committee Member
(Department of Electrical and Computer Engineering)

ABSTRACT

Smart meters (SMs) are key components of the smart grid (SG) as they gather electrical usage data from residences and businesses. Home area networks (HANs) are used to provide two-way communications between SMs and devices within a building such as appliances. This can be implemented using power line communications (PLCs) on home wiring topologies. In this thesis, a HAN PLC channel model is designed based on a split-phase power system which includes branch circuits, a panel with circuit breakers and bars, a secondary transformer and the wiring of neighboring residences. A cell division (CD) method is employed to construct the channel model. Further, arc fault circuit interrupter (AFCI) and ground fault circuit interrupter (GFCI) circuit breaker models are developed. Several PLC channels are presented and compared with those obtained using existing models. PLC communication systems are affected by noise, thus a noise model is developed which is comprised of background and impulse noise. This noise model can be used to obtain the noise power spectral density (PSD) at receivers in the wiring topology.

Contents

Supervisory Committee **ii**

Abstract **iii**

Table of Contents **iv**

List of Tables **vi**

List of Figures **vii**

List of Abbreviations **ix**

1 Introduction **1**

1.1 Power Line Communications for Home Area Networks 2

1.2 Organization of the Thesis 4

1.3 Contributions 5

2 HAN Topology Modeling **6**

2.1 Wiring Topology 6

2.2 Modeling Branch Circuits and Above the Panel 9

2.3 Modeling the Topology Inside the Panel 15

2.4 Cell Division Method 16

3 Model Analysis And Validation **23**

3.1 Topology Parameters 23

3.2 Channel Modeling and Analysis 24

3.3 Comparison of Channel Models 28

4 Noise Characterization **33**

4.1 Noise Modeling Examples 35

4.1.1 Background Noise 35
4.1.2 Impulse Noise 36

5 Conclusions **40**

A The Inner Self Inductance of a Circular or Rectangular Conductor **42**

Bibliography **45**

List of Tables

Table 2.1 Appliance Parameters 9
Table 2.2 Properties of Conductors 11
Table 2.3 Parameters of Rectangular Conductors in the Panel 16

Table 3.1 Parameters for the Three House Sizes 25
Table 3.2 Average IL for the Three House Sizes 26
Table 3.3 Average IL of the Three Parts of the Home Topology 28
Table 3.4 Parameters for Three Appliances 29

Table 4.1 Distribution of a 35
Table 4.2 Distribution of f_i 37
Table 4.3 Impulse Noise Parameters 37
Table 4.4 Power Spectral Density Differences Between (4.3) and (4.6) at the Impulse Noise Peaks 38

List of Figures

Figure 1.1 The average power consumption of residences. 2
Figure 1.2 An impedance carry back method [23] example. 4

Figure 2.1 The topology above the panel which includes the smart meter. 7
Figure 2.2 The topology of a 200 A Homeline panel. 8
Figure 2.3 AWG 6, 3 and 2/0 conductor strands. 11
Figure 2.4 Homeline breakers with ratings (a) 200 A and (b) 30 A and 20 A. . . 17
Figure 2.5 The circuit breaker model. 18
Figure 2.6 Impedance computation directions of the CD method. 19
Figure 2.7 A small appliance circuit cell. 20
Figure 2.8 The steps for cell modeling using the cell division method. 21
Figure 2.9 A simple topology divided into cells. 22

Figure 3.1 The IL of 15 channels from two different medium size house topologies. 26
Figure 3.2 The average IL of the channels in the 1000 topologies for each house size. 27
Figure 3.3 Average IL of the three parts of the home topology. 27
Figure 3.4 The average IL of the 9000 individual circuit channels and the 8000 SA circuit channels in the 1000 topologies. 28
Figure 3.5 The average IL with normal breakers and AFCI and GFCI breakers. . 29
Figure 3.6 The Cañete wiring topology modeled using (a) the ABCD matrix method, and (b) the cell division method. 30
Figure 3.7 The impedances of the three appliances. 31
Figure 3.8 The TFs of four conductors. 32
Figure 3.9 The TFs obtained using the ABCD and cell division methods. 32

Figure 4.1 The classification of PLC noise [51]. 34
Figure 4.2 Impulse noise characterization. 34

Figure 4.3 The best and worst cases of background noise. 36
Figure 4.4 (a) The PSD of the noise at the receiver, and (b) the corresponding CDF. 39

Figure A.1 Circular conductors when (a) the skin depth is greater than the radius, and (b) otherwise. 42
Figure A.2 A rectangular conductor when (a) the skin depth is greater than half the smaller of the width W and depth T, and (b) otherwise. 43

List of Abbreviations

2PN	Two-Port Network
AFCI	Arc Fault Circuit Interrupter
AWG	American Wire Gauge
AWGN	Additive White Gaussian Noise
BB	BroadBand
BB-PLC	BroadBand Power Line Communication
BPL	Broadband over Power Line
BPSK	Binary Phase Shift Keying
BSL	Bedroom, Study and Living Room
CD	Cell Division
CDF	Cumulative Distribution Function
CSMA	Carrier Sense Multiple Access
CSMA/CA	Carrier Sense Multiple Access with Collision Avoidance
CTF	Channel Transfer Function
DAC	Data Acquisition Center
DER	Distributed Energy Resource
DOE	Department Of Energy
FSK	Frequency Shift Keying
GFCI	Ground Fault Circuit Interrupter
HAN	Home Area Network
HVAC	Heating, Ventilation and Air Conditioning
ICB	Impedance Carry Back
IL	Insertion Loss
J-J	Junction To Junction
J-U	Junction To Unknown
LPTV	Linear Periodically Time Varying
LTI	Linear Time Invariant
MAC	Media Access Control

List of Abbreviations

MISO	Multiple-Input Single-Output
MIMO	Multiple-Input Multiple-Output
NB	NarrowBand
NB-PLC	NarrowBand Power Line Communication
NEC	National Electric Code
OFDM	Orthogonal Frequency Division Multiplexing
p.u.l.	Per Unit Length
PDF	Probability Density Function
PLC	Power Line Communication
PSD	Power Spectral Density
QOS	Quality of Service
RMS	Root Mean Square
RTP	Real Time Pricing
Rx	Receiver
S-FSK	Spread Frequency Shift Keying
SA	Small Appliance
SER	Service Entrance Cable
SG	Smart Grid
SH	Smart Home
SISO	Single-Input Single-Output
SIMO	Single-Input Multiple-Output
SM	Smart Meter
SMPS	Switched-Mode Power Supply
SS	Spread Spectrum
std	Standard Deviation
TDMA	Time Division Multiple Access
TF	Transfer Function
Tx	Transmitter

Chapter 1

Introduction

Increasing energy demands have resulted in increased greenhouse gas emissions. Governments are now taking efforts to combat climate change and adjust to its effects [1]. One of the approaches is to modernize the electric grid infrastructure and use renewable energy sources [2]. These distributed energy resources (DERs) require communication channels for the management of power transmission and distribution. A power grid with communication techniques to meet these purposes is often referred as a smart grid (SG) [3–5]. Smart meters (SMs) are part of the smart grid which are deployed at residences in place of traditional electric meters.

In North America and Europe, the legislative approval of smart meters has led to an increase in the number of intelligent devices such as smart appliances with a growing market of billions of dollars [6, 7]. One of the purposes of SMs is to help both power suppliers and residence owners with power management. Figure 1.1 shows the average power consumption of residences according to the survey by U.S. Department of Energy (DOE) in September 2017. The appliances for heating, ventilation and air conditioning (HVAC) and water heating account for approximately half of the power consumed. A smart meter installed in a residence can provide flexibility in managing these appliances to reduce costs.

Smart meters employ bidirectional communications in a smart grid. They can transmit data to data acquisition centers (DACs) for analysis and receive real time pricing information from the DACs. In a home area network (HAN), SMs collect power usage data from home appliances, send commands to control these appliances, and exchange information with the home owners. Real time pricing (RTP) can be implemented according to recommendations by power suppliers so appliances such as dishwashers, washing machines and dryers can be scheduled to operate during off-peak times when prices are low [8]. HVACs and water heaters can be run according to RTP either. Energy theft prevention is another

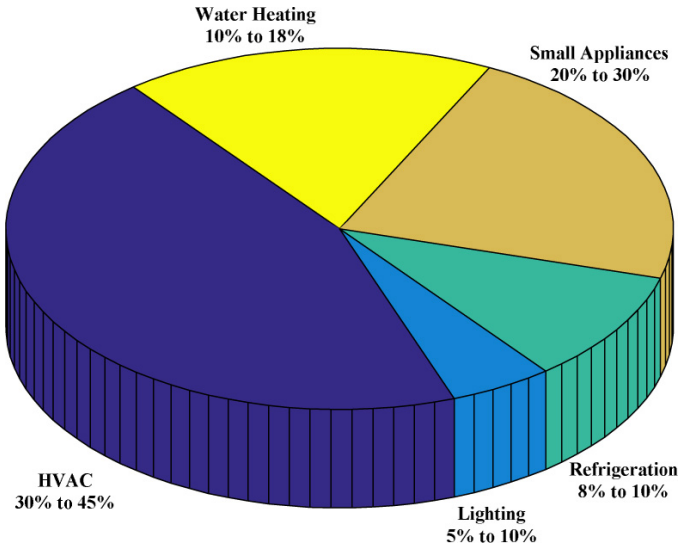

Figure 1.1: The average power consumption of residences.

function of SMs. With advanced theft detection and encryption algorithms, SMs can detect and report, as well as prevent illegal electricity usage [9]. Appliance monitoring can also be provided by regularly checking and reporting the status of appliances. SMs also benefit power suppliers as remote meter reading is more cost effective than manual reading.

1.1 Power Line Communications for Home Area Networks

The growing interest in smart home (SH) services has prompted research on broadband power line communication (BB-PLC) for high-speed data transmissions. IEEE Std 1901-2010 provides networking protocols for broadband over power line (BPL) devices [10]. IEEE Std 1901.2-2013 for narrowband power line communication (NB-PLC) assures co-existence with the broadband standard [11]. NB-PLC is suitable for the collection of power usage data, and so can be used to provide SM services within businesses and residences via HANs. Modulation schemes for PLC communications include binary phase shift keying (BPSK), frequency shift keying (FSK), spread frequency shift keying (S-FSK), spread spectrum (SS), orthogonal frequency division multiplexing (OFDM) or a combination of these techniques [12]. Media access control (MAC) protocols include carrier sense multiple access (CSMA) with collision avoidance (CSMA/CA) and time division multiple access (TDMA). Single-input single-output (SISO), single-input multiple-output (SIMO), multiple-input single-output (MISO) and multiple-input multiple-output (MIMO) techniques have been developed for wireless systems, but are not included in the IEEE BB-PLC and NB-

PLC standards.

Previous research on PLC based smart metering has focused on the links between SMs and DACs [13–16]. However, there has been little research on PLC for HANs. Thus, further study is required. Complex home wiring topologies can be characterized using the components to obtain accurate channel models. Several channel models have been proposed in the literature for this purpose. In [17], a channel model was developed based on a National Electrical Code (NEC) compliant topology. However, the model was constructed as a cascaded two-port network (2PN) with the same path loss in the phase and neutral conductors, which is not realistic. In [18–20], a model of a PLC system with a panel was given, but within the panel, only the bonding strap to the ground was included, so this model is incomplete. The model in [21] used the physical characteristics of conductors, appliances and outlets. However, only part of the panel was considered along with five branch circuits, which is insufficient to model a HAN network. In [22], the influence of circuit breakers on PLC channel models was investigated. Both normal and ground fault circuit interrupter (GFCI) breakers were considered. However, results were based using only measurements and so the results are not general.

The impedance carry back (ICB) method in [23] can be used to develop a HAN channel model. Figure 1.2 shows the steps of this method for a simple example. The backbone refers to the direct path between the transmitter and receiver, while the outlets o_1, o_2 and o_3, and nodes n_1 and n_2 are on an indirect path which is connected to the backbone at n_b. The impedance of this path is calculated from o_1 and o_2 to n_2, and finally to n_b as illustrated in Figs. 3(a) to 3(c). The use of indirect paths in developing a channel model is impractical for large topologies with a long backbone and many indirect paths. In this thesis, a simple and flexible method is developed which can be used for any topology. A cell division (CD) method is implemented for a split-phase power system and the structure includes both 120 V single phase and 240 V split phase circuits. This structure is used in North American residences. The panel is fully described unlike the approaches in [18–20, 22–24]. Further, models for arc fault circuit interrupter (AFCI) and GFCI circuit breakers are presented. A bottom-up approach [25] is employed so the topology is modeled from the individual components. The advantage is that once a topology is modeled, it can be used to develop models for other topologies.

Indoor power lines were not originally designed for communication purposes, and the influence of electromagnetic noise can be considerable. It was stated in [10, 11] that noise will have a significant effect on the PLC performance, including the reliability and the quality of service (QOS), and so is a primary concern in PLC systems. At present, noise

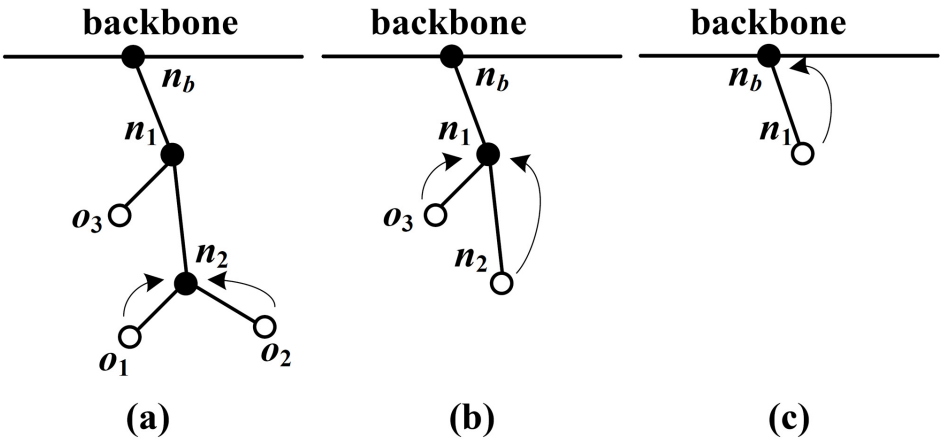

Figure 1.2: An impedance carry back method [23] example.

analysis has focused on the network between SMs and DACs [13–16], whereas the HAN has had less attention. The power line channel cannot simply be considered as an additive white Gaussian noise (AWGN) environment [51]. Therefore, the noise modeling for HAN channels is challenging. The noise varies with frequency [26], and can be considered from broadband [27–30] or narrowband perspectives [31–34]. Further, most noise modeling has employed only measurement results in a top-down approach. However, this approach is based on empirical results that only fit a specific topology, while a bottom-up approach is general and can be used in developing a variety of models. Thus, a noise model using the latter approach is proposed for HANs.

1.2 Organization of the Thesis

The remainder of this thesis is organized as follows.

Chapter 2 provides an overview of PLC channel modeling. A wiring topology is characterized using North American residences and standards. The parameters of components in the topology are obtained to determine the impedances. These impedances are used to compute the transfer functions of PLC channels. The CD method for channel characterization is described in detail.

Chapter 3 uses the CD method to develop HAN channel models and is compared with other approaches in the literature. Models are given for three house sizes, small, medium and large with floor areas of 1000, 2000 and 4000 ft^2, respectively. The smart meter is considered as the transmitter and modems in the branch circuits are

the receivers. Several branch circuits and breaker types are considered and their influence on the channel is examined. The CD method is implemented for a simple topology and the results are compared with those of existing methods.

Chapter 4 presents a HAN noise model which is comprised of background noise and impulse noise. The PSD of the noise at the receiver is obtained using the CD approach. The results obtained indicate that the proposed noise model is adequate for HANs.

Chapter 5 provides some concluding remarks and suggestions for future work.

The Appendix presents the inner self inductance of circular and rectangular conductors considering the skin effect.

1.3 Contributions

This thesis contributes to the area of power line communications in the context of home area networks. A wiring topology is modeled for North American residences with a split-phase power supply. A smart meter is considered as the PLC transmitter or receiver, which is seldom discussed in existing channel models. The parameters of the topology components are found and their impedances are derived. The channel transfer functions are obtained using these impedances. A cell division method is developed for channel characterization. Compared to other channel modeling methods, the cell division is simpler and can be used to model any wiring topology including those that are large and complex. The channel model obtained is compared with those in the literature to verify its accuracy. A noise model is also developed using this approach, and the noise power spectral density (PSD) at the receiver is obtained and compared with an existing model. This represents a new means of PLC noise modeling.

Chapter 2

HAN Topology Modeling

Home wiring topologies can be used for PLC data transmission. They can be modeled based on the NEC and American Wire Gauge (AWG) [35] standards. In this chapter, the wiring topology of a single 2000 ft^2 dwelling is developed. The parameters of the components within this topology are presented. A technique to model the topology is developed which can be used to obtain HAN channel models.

2.1 Wiring Topology

A home topology can be divided into three parts, the topology above the SM, the electrical panel up to the SM and the branch circuits. Figure 2.1 shows the topology above the panel. A secondary transformer delivers power to residences using a three-conductor service entrance cable (SER) [17] with AWG 4/0 conductors. From this cable, a SER with AWG 2/0 conductors is connected to the panel through the meter. The SERs above and below the SM are labeled L_B and L_A, respectively. L_A is between the smart meter and the junction with the AWG 4/0 conductors that connects residences to the transformer. L_{a_1}, L_{a_2} and L_{a_3} are the conductors in L_A that correspond to phase one, neutral and phase two, respectively. L_B is between the smart meter and the panel where L_{b_1}, L_{b_2} and L_{b_3} correspond to L_{a_1}, L_{a_2} and L_{a_3}.

The second part of the home topology is shown in Figure 2.2, which is a Homeline panel with a 200 A rating [36]. L_{b_1} and L_{b_3} connect the main breaker to the corresponding hot bars, where 120 V single-pole and 240 V double-pole circuit breakers are placed and connected to phase conductors in the branch circuits. L_{b_2} connects to a bonding strap which has the neutral bars on the ends. An AWG 6 bare conductor extends from the bonding

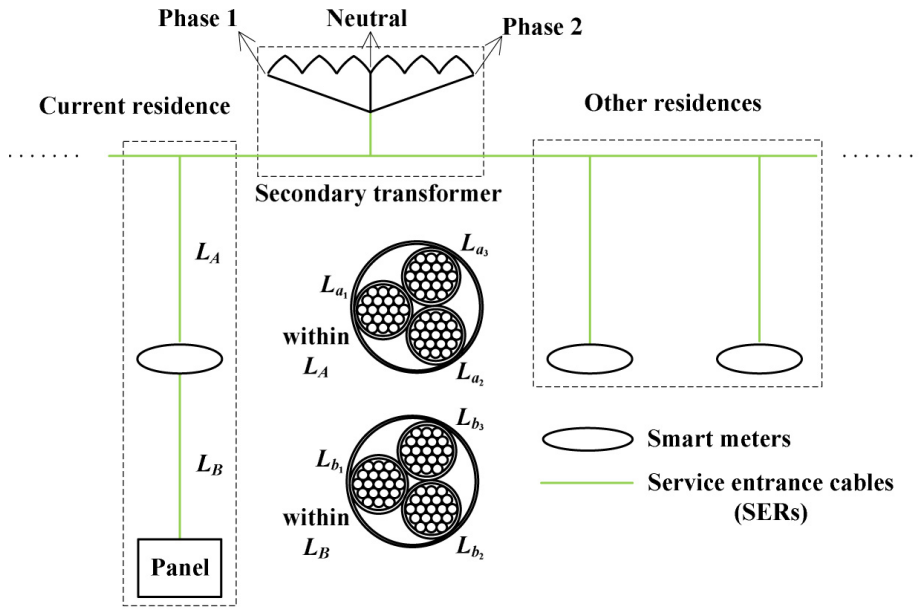

Figure 2.1: The topology above the panel which includes the smart meter.

strap to a ground rod, so the neutral bars have zero potential. Both the neutral and ground conductors are connected to the neutral bars.

The third part of the home topology is the branch circuits. They are extended from the panel and deliver power to appliances. Modems are connected to outlets to provide information about the associated devices. AWG 6, 8, 10, 12 and 14 refer to the most commonly used conductors in home wiring which correspond to 50, 40, 30, 20 and 15 A branch circuits, respectively. An 80% ampere rating of branch circuits is used for safety operation. For instance, the maximum current in a 50 A circuit is 40 A. The minimum number and maximum length of branch circuits, number of outlets on a branch circuit and distance between the outlets are given by NEC either. Branch circuits are classified as individual, lighting and small appliance circuits as follows.

An individual circuit supports an outlet for one electric appliance which typically has large power consumption. Individual circuits can be either split-phase or single-phase. The former type supports high power electrical appliances such as a range, range top, washing machine, dryer, HVAC or water heater that are above 2000 VA. The latter type supports appliances with comparatively lower power consumption such as a range hood, dishwasher, waste disposal and trash compactor, but large initial power is necessary to start the motors inside the appliances.

Lighting circuits are assumed to utilize fluorescent lamps or incandescent lamps with

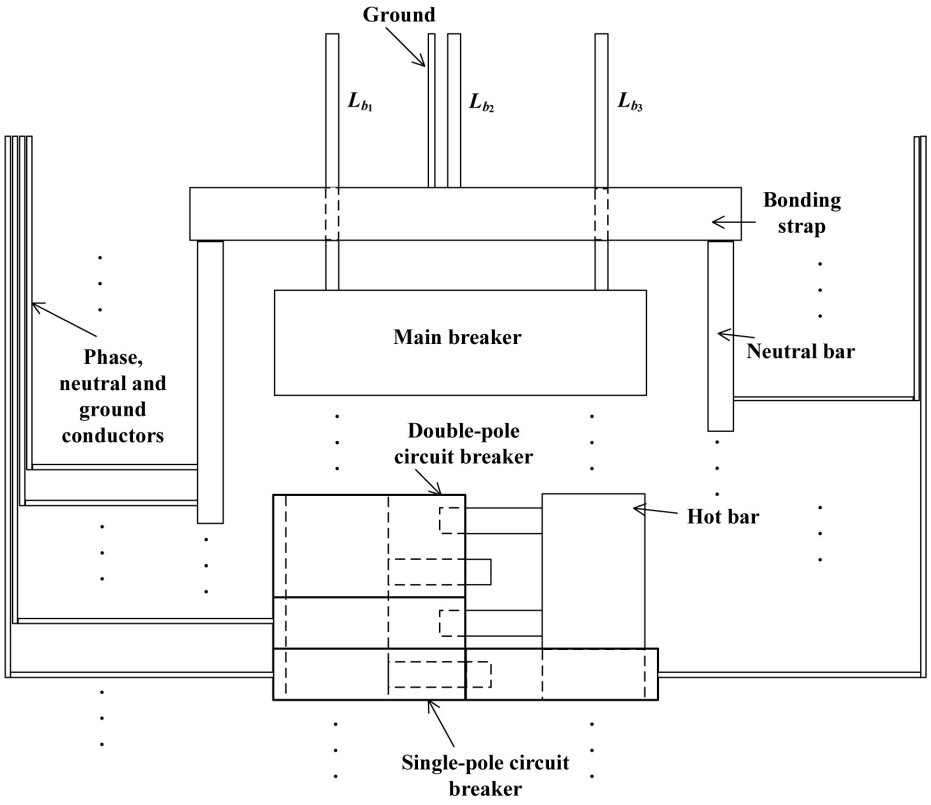

Figure 2.2: The topology of a 200 A Homeline panel.

switches to control them. At least one switch controlled light is required in each habitable room as well as bathrooms, hallways, stairways, garages, and storage or equipment spaces including attics, underfloor spaces, utility rooms, and basements. The floor area is calculated using the outside dimensions of the building to determine the required lighting power.

Small appliance (SA) circuits have multiple outlets for plug-in appliances other than those on individual circuits. These and all the other home appliances considered here are given in Table 2.1 [37]. They can be classified as resistive, reactive or linear periodically time varying (LPTV) (types 1 to 3, respectively) [25]. LPTV appliances have either commuted (3-1) or harmonic (3-2) impedance variations. There are seven types of circuits (a to g), which are split phase individual circuits, single phase individual circuits, lighting circuits, kitchen SA circuits, bedroom, study and living room (BSL) SA circuits, laundry area SA circuits and bathroom SA circuits, respectively. P_r is the power consumed by the appliance.

Table 2.1: Appliance Parameters

Appliance	Type	Circuit	P_r (VA)
Range	1, 2	a	8000 to 12000
Range top	1, 2	a	4000 to 6000
Range hood	2	b	70 to 240
Dishwasher	2	b	1200 to 1800
Waste disposal	2	b	300 to 800
Trash compactor	2	b	300 to 600
Dryer and washing machine	2	a	3000 to 5000
HVAC	2	a	2000 to 5000
Water heater	1, 2	a	2000 to 4000
Fluorescent lamp	3-1	c	20 to 100
Incandescent lamp	1	c	100 to 200
Live clock	2	d, e, f, g	5 to 15
Electric shaver	2	g	15 to 100
Smart phone charger	2	e	15 to 100
Blender	2	d	100 to 300
Stereo	3-2	e	100 to 300
Laptop	3-2	e	100 to 300
Plasma or LCD TV	3-2	e	100 to 300
Radio tuner	3-2	e	100 to 300
Humidifier	2	d, e, f, g	300 to 1000
Dehumidifier	2	d, e, f, g	300 to 1000
Refrigerator	3-2	d	300 to 1000
Percolator	1, 2	d	1000 to 1500
Toaster	1, 2	d	1000 to 1500
Potable kettle	1, 2	d	1000 to 1500
Iron	1, 2	e, f	1000 to 1500
Hairdryer	2	e, g	1000 to 1500

2.2 Modeling Branch Circuits and Above the Panel

PLC channels can be modeled using either a top-down approach or a bottom-up approach. Top-down channel models are based on parameters from extensive measurements [25]. Since wiring topologies differ, these results are typically not suitable for other channels. Further, measurement errors reduce the model accuracy. On the other hand, a bottom-up approach uses the actual wiring topology parameters to construct a model. Since the components can easily be changed, this technique is general and can be used for any topology [25]. In this section, a review of the component parameters is given. These parameters

are then used to develop the channel model for a topology.

The per unit length (p.u.l.) resistance R, inductance L, reactance G and capacitance C of conductors are considered first. These parameters are determined by the physical properties of conductors [35], including the material (copper or aluminum), the number and diameter of conductors in cables and strands in conductors, as well as the material and thickness of the conductor insulation. The p.u.l. resistance of a conductor R is derived from

$$R = \frac{\rho}{A} \tag{2.1}$$

where the cross section area A is related to skin depth $\delta = \frac{1}{\sqrt{\pi\mu\sigma f}}$ and f is the frequency. For a circular conductor with radius r, if $\delta \geq r$ as in Appendix Figure A.1a, $A = \pi r^2$. If $\delta < r$ as in Appendix Figure A.1b, $A = \pi[r^2 - (r-\delta)^2] = \pi\delta(2r - \delta)$. μ is the magnetic permeability. For copper or aluminum, μ is equal to the vacuum magnetic permeability $\mu_0 = 4\pi \times 10^{-7}$ H/m. The conductivity σ is inversely proportional to the resistivity of material ρ, which is 2.15×10^{-8} Ωm for copper, and 3.45×10^{-8} Ωm for aluminum [35]. For simplicity, frequency dependent variables are expressed without the frequency variable, i.e. $R(f)$ is denoted as R. The p.u.l. resistance of a circular conductor is expressed as

$$R = \begin{cases} \dfrac{1}{\pi\sigma r^2} & \text{when } \delta \geq r, \\ \dfrac{1}{\pi\sigma\delta(2r-\delta)} & \text{when } \delta < r, \end{cases} \tag{2.2}$$

The copper conductors are used in modeling and the properties are given in Table 2.2. The number of conductors in a cable is used to infer the central distance of the paired conductors for the channel. In a 3-conductor cable, the central distance of two adjacent conductors is the diameter of a single conductor with its insulation. In a 4-conductor cable, the paired conductors can be in adjacent or diagonal positions [18], and the central distance in the first position is the same as the 3-conductor cable given the same conductors, and differs by a factor of $\sqrt{2}$ in the second position. The conductor insulation can be either polythelene or nylon polyamide and this determines the capacitance of the conductors. The insulation thickness and diameter of a bare conductor are used to infer the central distance of adjacent conductors. DC resistance values are used in voltage drop calculations to determine the length of conductors.

For conductors with more than one strand, i.e. 7 strands for AWG 3 and 6 and 19 strands for AWG 2/0 and 4/0 as shown in Figure 2.3, the current is concentrated in the outer ring of

Table 2.2: Properties of Conductors

Properties	Cable type						
	XHHW	SER	NM-B				
AWG	2/0	3	6	8	10	12	14
Number of conductors in cable	3	3	4	4	4	3	3
Material of conductor insulation	Polythelene		Nylon Polyamide				
Relative dielectric constant ξ_r	2.3		2.55				
Insulation thickness (mil)	55	45	35	35	24	19	19
Diameter of bare conductors (mm)	10.62	6.60	4.67	3.264	2.588	2.05	1.63
Strand diameter (mm)	2.13	2.20	1.56				
Number of strands: total/outer ring	19/12	7/6	7/6				
DC resistance (ohm/kft)	0.0967	0.245	0.491	0.764	1.21	1.93	3.07

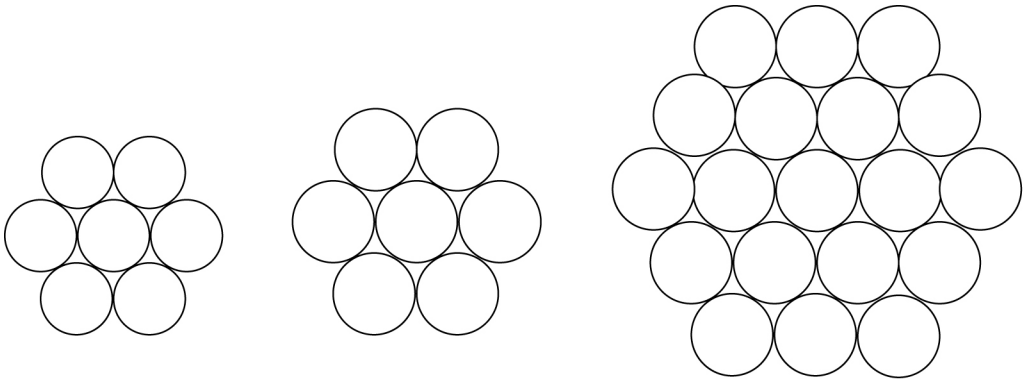

Figure 2.3: AWG 6, 3 and 2/0 conductor strands.

strands. For these conductors, the resistance R is multiplied by a correction factor [40, 41]

$$X_R = n_e \frac{r_s^2 \cos^{-1}\left(\frac{r_s - \delta}{r_s}\right) - (r_s - \delta)\sqrt{r_s^2 - (r_s - \delta)^2}}{2r\delta} \tag{2.3}$$

where the number of strands in the outer ring of conductors n_e and strand radius r_s are given in Table 2.2.

For a pair of conductors, the inductance is

$$L = L_{in} + 2(L_{out} \pm M) \tag{2.4}$$

which is comprised of inner self inductance L_{in}, outer self inductance L_{out} and mutual

inductance M. In common mode M is added to L_{out} and differential mode M is subtracted from L_{out}. Differential mode is preferred in PLC as the common mode noise is neutralized [36]. so

$$L = L_{in} + 2(L_{out} - M) \tag{2.5}$$

is used in this thesis. If $\delta \geq r$, $L_{in} = \dfrac{\mu}{8\pi}$ [38]. When $\delta < r$, L_{in} of a circular or rectangular conductor is given in the Appendix. If the conductor length l is much greater than the radius r and central distance d, then

$$L_{out}(l) = \frac{\mu}{2\pi}\left(\log_{10}\frac{2l}{r} - 1\right) \tag{2.6}$$

$$M(l) = \frac{\mu}{2\pi}\left(\log_{10}\frac{2l}{d} - 1\right) \tag{2.7}$$

and the inductance L is

$$L = \begin{cases} \dfrac{\mu}{\pi}\log_{10}\left(\dfrac{d}{r}\right) + \dfrac{\mu}{8\pi} & \text{when } \delta \geq r \\ \dfrac{\mu}{\pi}\log_{10}\left(\dfrac{d}{r}\right) + \dfrac{\mu}{8\pi}(1-(1-\dfrac{\delta}{r})^4) & \text{when } \delta < r \end{cases} \tag{2.8}$$

In a homogeneous dielectric environment, the p.u.l. capacitance and reactance can be obtained from [40]

$$\begin{aligned} LC &= \mu\xi \\ LG &= \mu\sigma \end{aligned} \tag{2.9}$$

where the dielectric constant is $\xi = \xi_0\xi_r$, $\xi_0 = 8.859 \times 10^{-12}$ F/m is the vacuum dielectric constant, and ξ_r is the relative dielectric constant which is 2.3 for AWG 2/0 to 3 conductors (polyethelene) and 2.55 for AWG 4 to 14 conductors (nylon polyamide). The p.u.l. parameters are used to obtain the characteristic impedance Z_c and propagation constant γ of the conductors [23]

$$Z_c = \sqrt{\frac{R + j\omega L}{G + j\omega C}}, \quad \gamma = \sqrt{(R + j\omega L)(G + j\omega C)}$$

where $\omega = 2\pi f$.

The end of a conductor furthest from the transmitter is called the input while the other end is called the output. The input impedance of a conductor Z_{in} is determined by the

impedance of all components at the input of the conductor. For instance, if the conductor is between an outlet and an appliance which is on, the impedance of the appliance is the input impedance. If the appliance is off or the outlet is open (i.e. no appliance), then Z_{in} = ∞. If Z_{in} is determined by N parallel impedances Z_1, Z_2, ..., Z_N, i.e. at the junction of several conductors or at an outlet with a modem and an appliance, then

$$\frac{1}{Z_{in}} = \frac{1}{Z_1} + \frac{1}{Z_2} + \cdots + \frac{1}{Z_N}. \tag{2.10}$$

NEC places limits on conductors in branch circuits [17] including the gauge of conductors, ampere rating of branch circuits, minimum number and maximum length of branch circuits, number of outlets on a branch circuit, and distances between outlets. The length of a branch circuit should accommodate a maximum 3% voltage drop [35]. For individual circuits, the voltage drop V_d of a conductor is [42]

$$V_d = 2R_s L_s I, \tag{2.11}$$

where R_s is the p.u.l. DC resistance of the conductor given in Table 2.2. The minimum length is $L_{min} = 6$ ft [37], and the maximum length L_{max} should be less than 100 ft. The maximum current I_{max} is 0.8 times the amperage rating of the corresponding circuit breaker. L_{max} can be obtained from (2.11) considering the maximum voltage drop. For lighting and small appliance circuits [21]

$$V_d = 2R_s \sum_{n=1}^{N} l_n I_n, \tag{2.12}$$

where N is the number of outlets. The maximum number of outlets is $N_{max} = \dfrac{I_{max}}{1.5}$ where the rated current of each outlet is 1.5 A [35]. The furthest outlet from the circuit breaker corresponds to $n = 1$, and l_n is the length of the conductor between outlets n and $n + 1$, or between outlet N and the circuit breaker [17]. $I_n = 1.5 \times n$. NEC recommends that for a branch circuit, the distance from the circuit breaker to the closest outlet should not exceed 70 ft for an AWG 12 conductor (SA circuit), or 50 ft for an AWG 14 conductor (lighting circuit). The recommended distance between outlets is 0 to 12 ft.

The output impedance of a conductor is [24]

$$Z_{out} = Z_c \frac{Z_{in} + Z_c \tanh(\gamma l)}{Z_c + Z_{in} \tanh(\gamma l)}, \tag{2.13}$$

and this is used as the input impedance of other conductors. The transfer function (TF) of a conductor is the ratio of the voltage at the input V_i to the voltage at the output V_o [17], and is given by

$$H = \frac{V_i}{V_o} = \frac{Z_{in}}{Z_{in}\cosh(\gamma l) + Z_c \sinh(\gamma l)} \tag{2.14}$$

Appliance impedances are the input impedances of the corresponding outlet conductors and are obtained as follows [25]. Resistive type appliances have negligible reactive impedance, so their impedances are constant values. Typical resistive appliances are heating loads such as an electric range, range top, water heater and electric kettle. The reactive components of these appliances, such as coils in small LEDs, are inductances smaller than 10^{-2} μH. An incandescent lamp has a coil inductance smaller than 1 μH. The impedance of resistive loads is

$$Z_{app} = \frac{U^2}{P_r}, \tag{2.15}$$

where $U = 120$ V for single phase and $U = 240$ V for split phase circuits.

Reactive type appliances have frequency-selective impedances. This includes inductive heating and appliances with motors such as hairdryers and air conditioners. The impedance of reactive loads is obtained from the parallel RLC circuit model [25] as

$$Z_{app} = \frac{R_s}{1 + jQ_f\left(\frac{\omega}{\omega_0} - \frac{\omega_0}{\omega}\right)} \tag{2.16}$$

where $R_s = \dfrac{U^2}{P_r}$ is the resistance at resonance. The quality factor Q_f is an indication of frequency selectivity and is typically between 5 and 25. The resonant frequency $f_0 = \dfrac{\omega_0}{2\pi}$ is between 25 kHz and 200 kHz [43, 44].

Linear periodically time varying type appliances have frequency-selective and time varying impedances. This includes fluorescent lamps, radio tuners, computers and smart TVs. The impedance variations of LPTV loads are caused by non-linear elements such as thyristors. These appliances can be described using the series linear time invariant (LTI) model given in [25].

A secondary transformer is included in the HAN model. It is connected to residences by overhead and underground SERs. In [45], impedance measurements of secondary transformers with capacities from 10 kVA to 50 kVA were given. From these results, the sec-

ondary transformer impedance is

$$Z_t = R_t + jX_t, \tag{2.17}$$

where at 0 Hz, R_t is between 0 and $1\ \Omega$ and X_t is $0\ \Omega$, and R_t and X_t increase with frequency at rates from 0.054 to $0.081\ \Omega$/kHz and 0.4 to $1\ \Omega$/kHz, respectively.

2.3 Modeling the Topology Inside the Panel

The conductors in the panel are modeled differently than in the rest of the topology because of their structure. In branch circuits and the topology above the panel, the conductors are closely packed in cables with the phase and neutral conductors sealed by insulation. The length l of these conductors is far greater than the cross section dimensions r and d. In the panel, the conductors are further apart and can be circular or rectangular. The latter type comprises bars and the bonding strap, which are not sealed, and the cross section dimensions are comparable to the lengths. The p.u.l. impedance of a conductor in the panel is

$$Z_{cp} = R_{cp} + jX_{cp}, \tag{2.18}$$

where R_{cp} is the p.u.l. resistance. For circular conductors, R_{cp} is the same as in branch circuits. For the rectangular case [46]

$$R_{cp} = \begin{cases} \dfrac{1}{\sigma WT} & \text{when } \delta \geq \min(W,T), \\ \dfrac{1}{2\sigma\delta(W+T-2\delta)} & \text{when } \delta < \min(W,T), \end{cases} \tag{2.19}$$

where W and T are the width and thickness of the conductor, respectively. The imaginary part of Z_{cp} is $X_{cp} = 2\pi f L_{cp}$ where $L_{cp} = L_{in} + L_{out}$ is the p.u.l. inductance. The corresponding TF is

$$H_{cp} = \frac{Z_{in}}{Z_{in} + Z_{cp}}. \tag{2.20}$$

The parameters of the rectangular conductors are summarized in Table 2.3.

Homeline thermal magnetic breakers are widely used in North America and are referred to as normal breakers. Three Homeline breakers are shown in Figure 2.4a and Figure 2.4b, which shows a 200 A main breaker and 30 A and 20 A circuit breakers, respectively. In the past 20 years, advanced Homeline AFCI or GFCI breakers have been developed to provide

Table 2.3: Parameters of Rectangular Conductors in the Panel

Conductor name	Size (in)		
	Width (W)	Thickness (T)	Length (l)
Hot bar slab	0.5	0.25	1.75
Hot bar	1.75	0.25	1 (central distance between slabs)
Neutral bar	0.3125	0.4375	0.3125 (central distance between slots)
Bonding strap	1	0.25	9

fault current detection and protection [47–49]. In [22], circuit breakers with various ampere ratings were modeled, but only single-pole normal breakers were considered. In this thesis, both single-pole and double-pole, normal and advanced Homeline circuit breakers are modeled.

Figure 2.5 shows the general model for a Homeline breaker. The normal breaker structure is shown on the left of the dashed line and includes a bare copper wire, a bimetallic strip using alloys of copper and steel, and a single copper strip. The bare copper conductor has a radius r determined by the breaker amperage and the length l is 2 in. The width and length of the strips are 0.5 and 1.75 in, respectively. In the main breaker, their thickness is 0.08 in, which in branch circuit breakers is 0.04 in. An AFCI or GFCI breaker includes the right part with coils and two conductors. One conductor of length 1.75 in connects the single copper strip to the phase conductor of the corresponding branch circuit. The other conductor of length 17.5 in connects the neutral conductor to the neutral bar. In an AFCI breaker, sensing coils T1 and T2 detect series and parallel arcing caused by loose connections and broken conductors, respectively. A GFCI breaker only has a T2 coil to detect parallel arcing. A double-pole circuit breaker can be considered as two parallel single-pole breakers. For AFCI or GFCI double-pole breakers, three conductors are used and monitored by the T1 and T2 coils. The impedance and transfer functions of the conductors within these breakers can be obtained using (2.13) and (2.14), or (2.18) and (2.20) with the parameters above.

2.4 Cell Division Method

In this thesis, the cell division method is introduced as an efficient means of modeling HAN topologies. This approach divides a topology into cells and determines the corresponding impedances and transfer functions. The appliances, modems and SM, conductors and secondary transformer are considered as basic components of the topology, and a cell

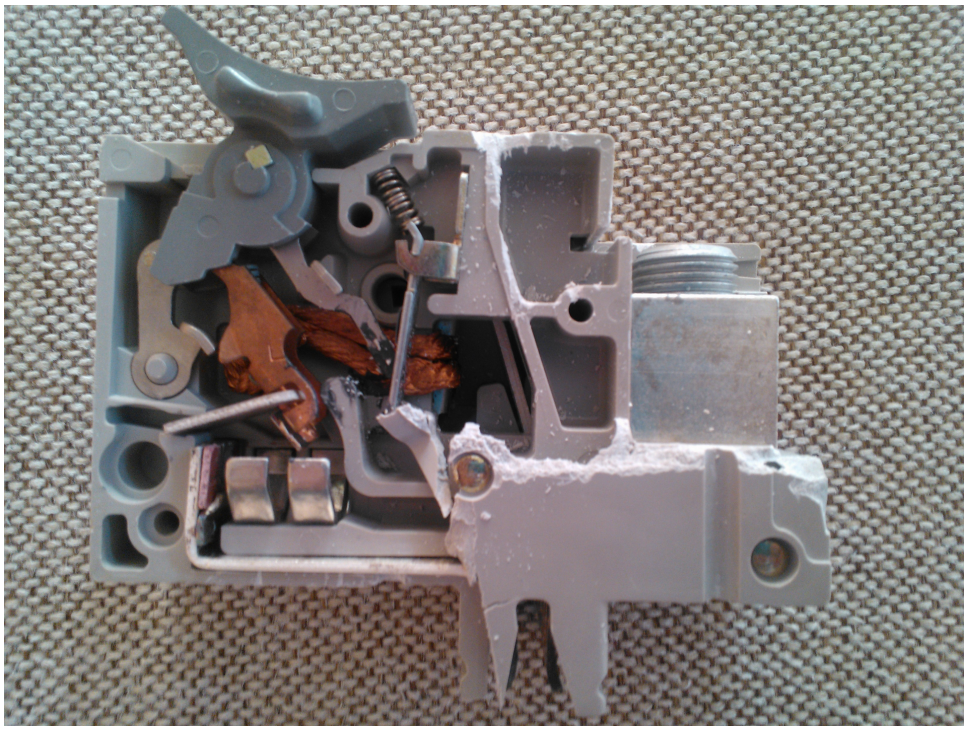

(a)

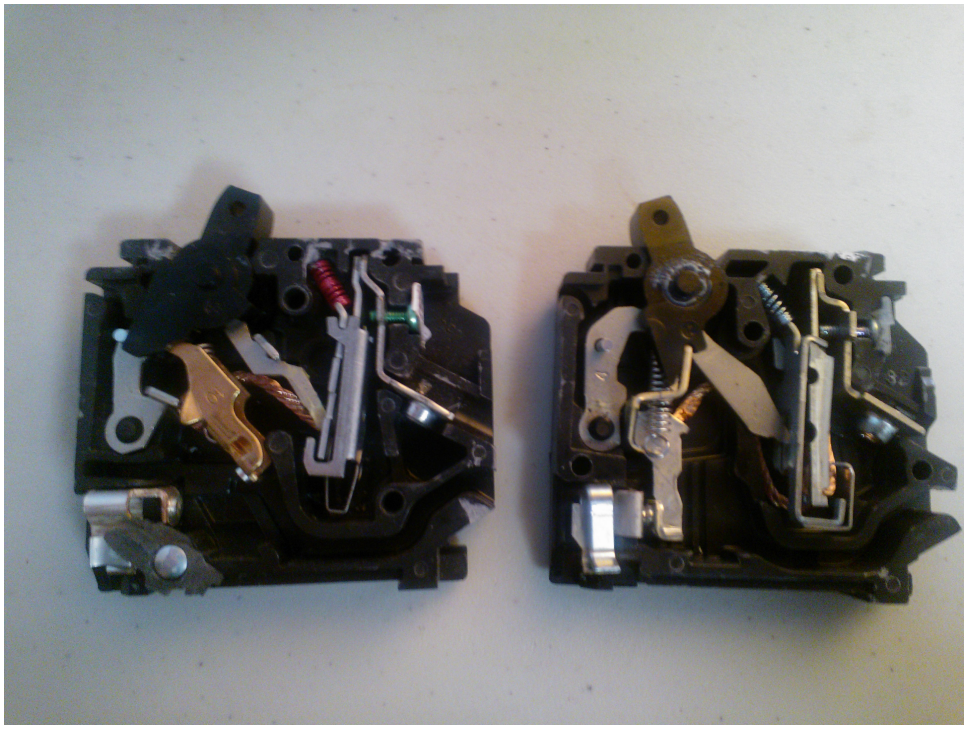

(b)

Figure 2.4: Homeline breakers with ratings (a) 200 A and (b) 30 A and 20 A.

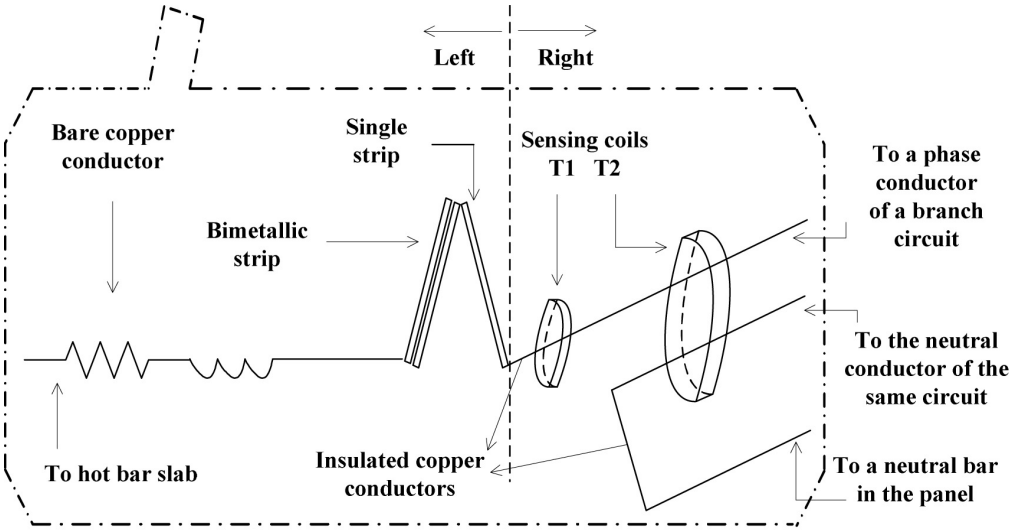

Figure 2.5: The circuit breaker model.

is comprised of several basic components. Each cell comprises only one junction, which is a node with three conductors. The conductors are divided into two groups, junction to junction (J-J) and junction to unknown (J-U). A cell comprises a junction, J-J and J-U conductors, and other components. A J-J conductor connects the cells of adjacent junctions. A J-U conductor is between a junction and other components such as an open outlet, an appliance with a modem, a single appliance, the smart meter, or another J-U conductor.

The CD method consists of the following steps. Once the topology is obtained, cells are defined and categorized into three types according to the conductors at the junctions. The first type are cells with one J-J and two J-U conductors such as those at the ends of the branch circuits. The second type are cells with two J-J and one J-U conductors such as those in the remainder of the branch circuits. The third type are cells with three J-J conductors such as those in the panel. Next, the Tx and Rx locations are determined which can be in the first and second types. The inputs and outputs of all the conductors are then determined. As shown in Figure 2.6, the impedance computation for cells is carried out following a bottom-up approach. For branch circuits without the Tx, the computation is from the first type cells to the third type cells (in the panel). The topology above the panel is similar to a branch circuit where the smart meter can be a Tx or Rx. For the branch circuit with the Tx, the computation continues to the Tx cell and ends when the output of the J-U conductor to the Tx is obtained.

Assume that the smart meter is the Tx. The TF of the topology below the SM is obtained

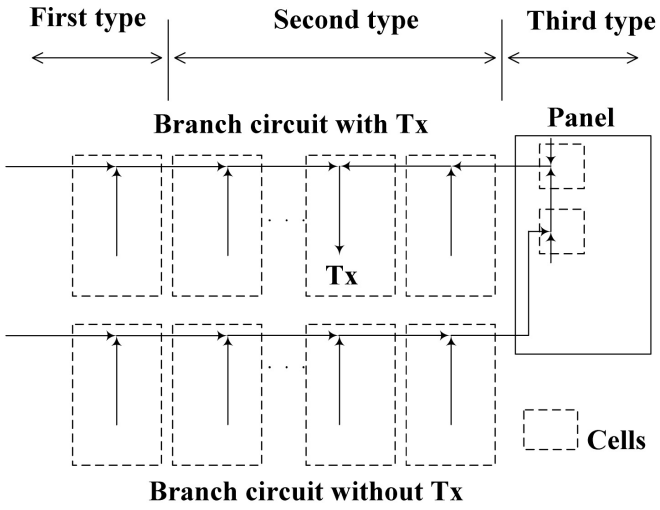

Figure 2.6: Impedance computation directions of the CD method.

using the corresponding impedances. The TF of paired conductors uses (2.14), whereas (2.20) is employed for single conductors in the panel. The TFs of the J-U and J-J conductors are denoted by H_{J-U} and H_{J-J}, respectively. Then

$$H_b = H_{J-U}(1)\left(\prod_{i=1}^{N_c-1} H_{J-J}(i)\right) H_{J-U}(N_c), \tag{2.21}$$

where $i = 1$ corresponds to the Rx cell and N_c is the number of cells in the direct path between the Tx and Rx. Next, the topology above the panel is considered as shown in Figure 2.1. If L_{b_1} and L_{b_2} are used which correspond to phase one and neutral, then the output impedance Z_b is obtained as the impedance of the current residence. The impedances Z_b of other residences are obtained using the same approach with a random but similar topology. Using this topology, the output impedance Z_a of L_A can be inferred using (2.13) which represents the impedance of the topology above the SM. The TF of the topology above and including the SM is

$$H_{as} = \frac{Z_a \parallel Z_b}{Z_a \parallel Z_b + Z_{sm}}, \tag{2.22}$$

where $\parallel$ denotes that the two impedances are in parallel, Z_{sm} is the impedance of the smart meter, which is the modem impedance assumed to be 50 Ω [25]. The TF for the complete topology is then

$$H_t = H_b \times H_{as}. \tag{2.23}$$

Figure 2.7 shows a cell on a small appliance circuit where l_1 and l_2 are the J-U con-

ductors to the appliance and outlet, respectively, and l_4 is the J-J conductor to the next cell. The procedure for determining the cell TFs is given in Figure 2.8. The outlet can be open, connected to an appliance, or to an appliance with a modem, and the appliance can be on or off. If the cell is furthest from the corresponding circuit breaker, then l_3 is connected to an outlet as a J-U conductor, and modeled with l_2 using the steps between the $*$ in Figure 2.8. Otherwise, l_3 is a J-J conductor so the input impedance of l_3 is obtained from the cell at its input. When the impedances of these conductors are obtained, the inputs of conductors l_2 and l_3 are examined to see if the Rx is present. If the Rx is at the input of l_2 or l_3, then it also an input of l_4, so the TFs of l_2 and l_4, or l_3 and l_4 are obtained. If there is no Rx, then only the impedances are necessary. Cells in the remainder of the topology are then modeled in turn using the same procedure. A simple topology which has been divided into cells is shown in Figure 2.9. For the given five cells, the impedance is computed rightwards in a bottom-up approach. In the process, only the TFs of denoted U-J and J-J conductors are computed.

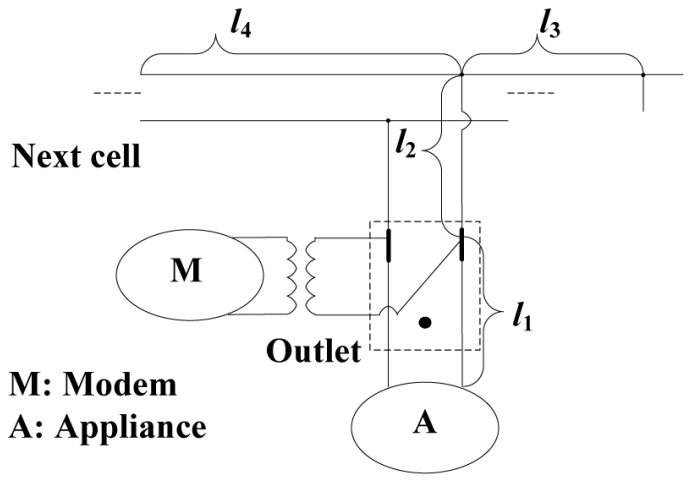

Figure 2.7: A small appliance circuit cell.

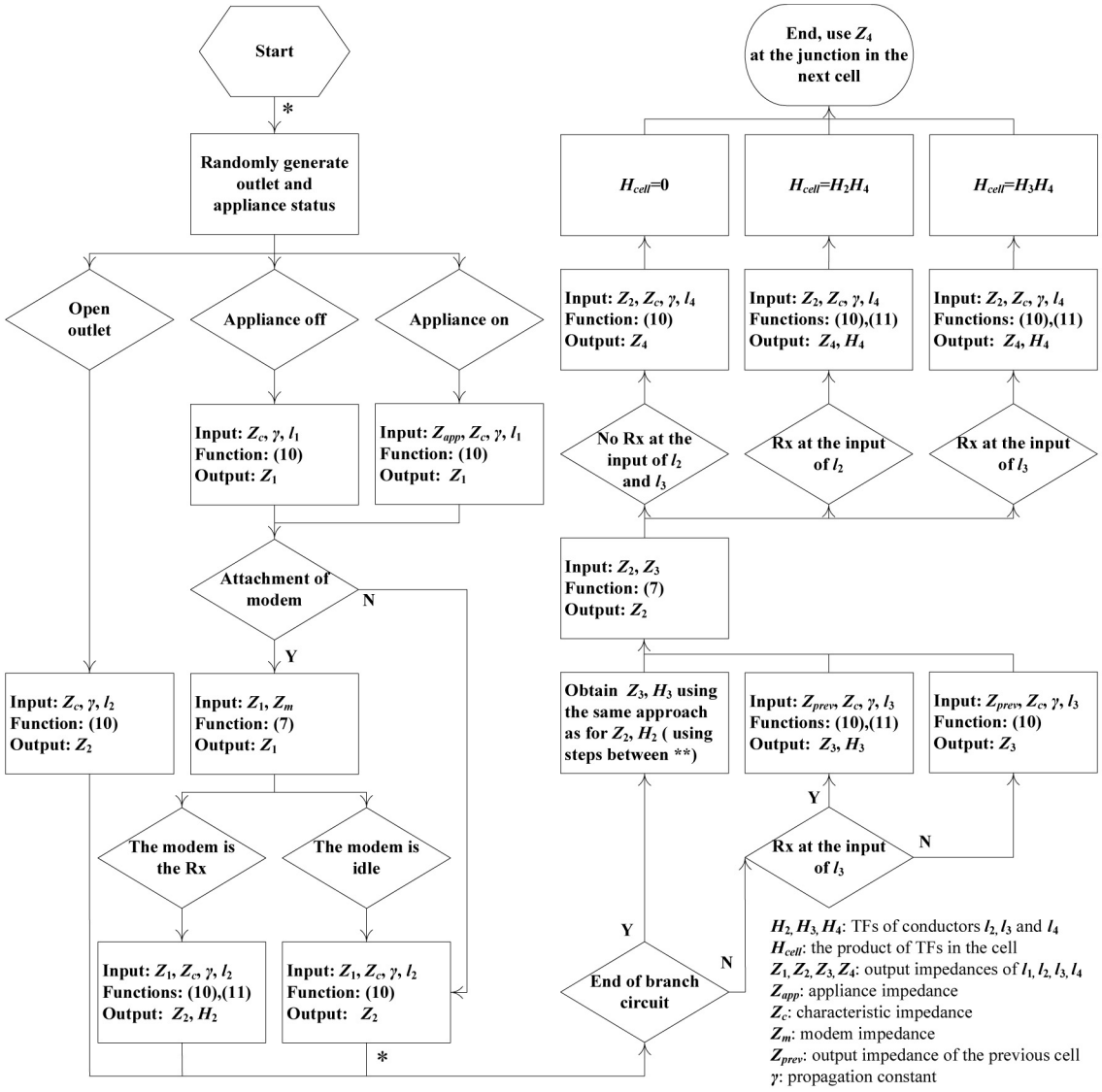

Figure 2.8: The steps for cell modeling using the cell division method.

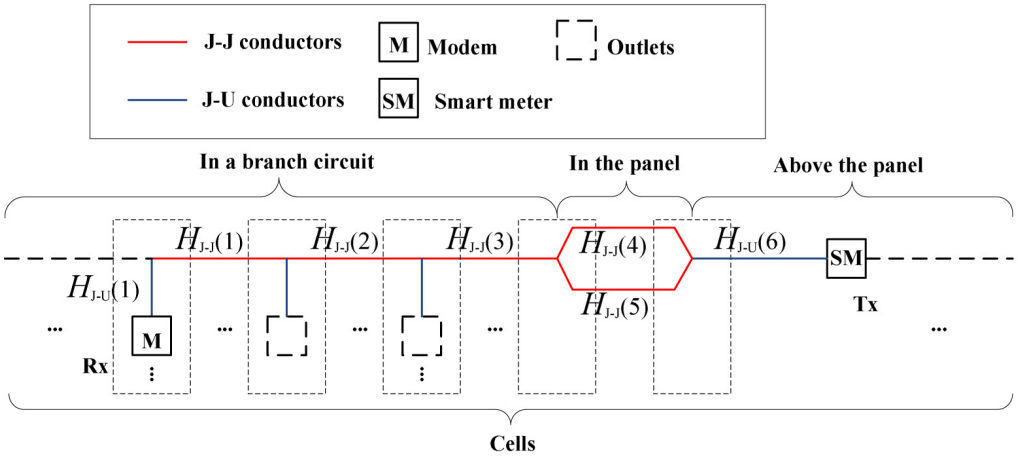

Figure 2.9: A simple topology divided into cells.

Chapter 3

Model Analysis And Validation

To obtain a channel model for a topology, a database of component parameters is used which includes the characteristic impedances and propagation constants of conductors, cross section areas of conductors in branch circuits, and the dimensions of the conductors in the panel. The IEEE low-frequency NB-PLC standard [11] for smart applications specifies a frequency band from 3 kHz to 500 kHz. The frequency-dependent parameters are determined for 256 discrete values uniformly distributed between these frequencies. In a topology, the SM is assumed to be the Tx and the Rx is a modem on a branch circuit. The TFs are determined for the channels to all modems in the topology.

3.1 Topology Parameters

All random parameters are obtained using a uniform distribution. The branch circuits are considered first and the appliances connected to them are either on or off with independent probabilities of 0.5. The lighting circuits are determined by the floor area. Consider a medium size house with a floor area of 2000 ft^2. According to NEC, the minimum lighting required is 3 VA/ft^2, so the minimum lighting load is 6000 VA. Lighting circuits are 120 V and 15 A, so the maximum load is $15 \times 80\% \times 120 = 1440$ VA where the 80% load rating is for overcurrent protection. The rating of an outlet is 180 VA, so there can be $1440/180 = 8$ outlets on a circuit. Thus 4 lighting circuits are required and AFCI breakers recommended. Another circuit with 4 lights for 2 bathrooms is assumed and in this case GFCI breakers recommended. Each light switch controls a fluorescent or incandescent lamp with equal probability.

The medium house is assumed to have 9 individual circuits for the appliances given in

Table 2.1 with circuit types a and b. There are 5 appliances of type a controlled by double-pole breakers and 4 of type b controlled by single-pole breakers. The power required is used to determine the size of the conductors and the amperage of the circuit breakers. Then Z_c and γ for the conductors in the topology are determined.

SA circuits correspond to circuit types d to g in Table 2.1 and each supports a maximum of $(20 \times 80\% \times 120)/180 \approx 10$ outlets for low power appliances. NEC suggests at least two circuits for kitchens, plus one for the laundry area and one for bathrooms. In the medium house model, two SA circuits each with 10 outlets are in the kitchen, and each bathroom and laundry circuit has 4 outlets. These are wet environments, so GFCI breakers are recommended. There are 8 different appliances which can be located on the two kitchen SA circuits, 3 on the laundry SA circuit and 4 on the bathroom SA circuit. Four bedrooms, a living room and a study are assumed with 5, 10 and 5 outlets in each room, respectively, which requires 4 SA circuits. There are 10 different appliances which can be located on these circuits. A TV, laptop and smart phone charger are randomly positioned in each room with independent probabilities of 0.5. One live clock is placed on a random SA outlet in the house. Further, one humidifier or dehumidifier with equal probability of 0.5 is randomly located on an SA circuit. An iron is located on a laundry or BSL SA circuit and a hair dryer is located on a bathroom or BSL SA circuit. The parameters for small, medium and large house sizes including the numbers of appliances are given in Table 3.1.

Within the panel, the circuit breakers are placed evenly on both sides of the hot bars starting from the top. The length of the cable (AWG 2/0) between the panel and the SM is between 6 ft and 10 ft. The cable (AWG 2/0) between the SM and junction to the transformer cable (AWG 4/0) is between 40 ft and 50 ft. There are between 5 and 20 residences randomly located on the transformer cable with from 50 ft to 70 ft between them. The secondary transformer is randomly located on the AWG 4/0 cable.

3.2 Channel Modeling and Analysis

The insertion loss (IL) can be expressed as

$$IL = 20 \log_{10} |H_t| , \tag{3.1}$$

where H_t is obtained from (2.23).

To better illustrate the impact of the topology components, first only normal breakers are considered. AFCI and GFCI breakers will be employed later. MATLAB was used to

Table 3.1: Parameters for the Three House Sizes

House size	Small	Medium	Large
Floor area (ft^2)	1000	2000	4000
Length of the branch circuits (ft)	6 - 80	6 - 100	6 - 150
Number of lighting circuits	4	5	10
Number of bathroom lights	2	4	6
Number of BSL SA circuits	2	4	6
Number of kitchen SA circuits	2	2	3
Number of laundry SA circuit outlets	2	4	6
Number of bathroom SA circuit outlets	2	4	6
Number of kitchen appliances	5 to 7	5 to 7	5 to 7
Number of BSL appliances	14 to 18	20 to 24	29 to 33
Number of laundry appliances	0 to 2	0 to 3	0 to 3
Number of bathroom appliances	1 to 2	1 to 4	1 to 4
HVAC	1500 to 3000 VA	2000 to 5000 VA	3000 to 7000 VA
Refrigerator	200 to 800 VA	300 to 1000 VA	500 to 1500 VA

obtain the transfer functions for 1000 random topologies of each of the small, medium and large house sizes. The execution times were 233 s, 322 s and 382 s, respectively. The average IL of the TFs for each size are given in Figure 3.2 and summarized in Table 3.2. The IL is highest for frequencies close to 0 kHz but decreases rapidly with frequency. The IL is lowest at 500 kHz, and fluctuates in the remaining frequency spectrum. The average IL of the small house is approximately 5.9 dB better than the medium house and 7.6 dB better than the large house. Thus, both the frequency and topology have a significant influence on the IL, and the larger the house the higher the IL.

Only the medium house is considered in the remainder of this chapter. Figure 4.4 shows the ILs of 15 different channels from two random medium house topologies. Although the magnitude varies, the channels have similar peaks and notches at certain frequencies. This is due to the same components within a topology. A home topology can be divided into three parts, the branch circuits, the panel up to the SM, and the SM and above. To better understand their effect on the channel, the average IL for each part is given in Figure 3.3 and summarized in Table 3.3. This indicates that the topology above the SM significantly affects the IL.

SA circuits and individual circuits are now compared. The average IL of the SA and individual circuit channels is shown in Figure 3.4. The average IL difference is between

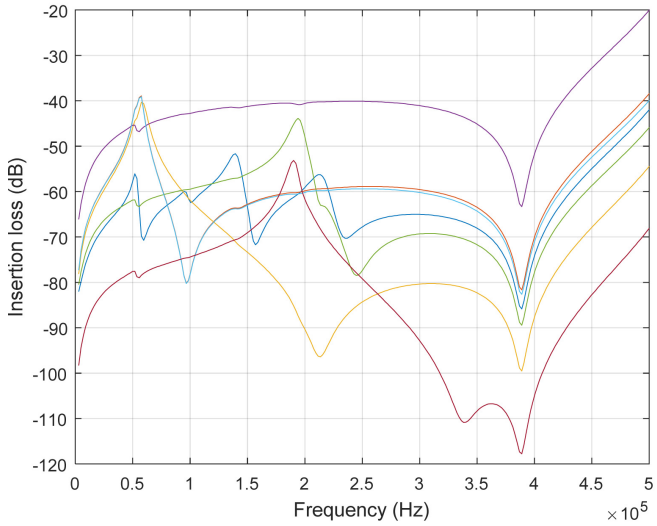

(a)

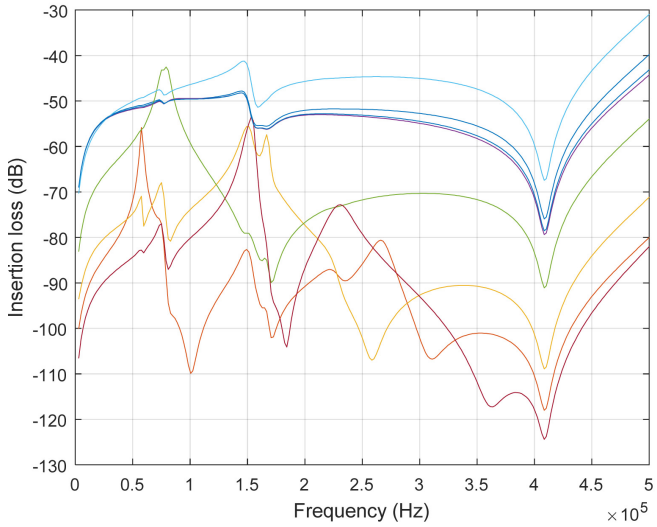

(b)

Figure 3.1: The IL of 15 channels from two different medium size house topologies.

Table 3.2: Average IL for the Three House Sizes

Size	Minimum (dB)	Maximum (dB)	Mean (dB)
Small	-77.31	-53.41	-59.64
Medium	-83.60	-59.30	-65.50
Large	-84.67	-60.71	-67.25

-17.0 dB and -8.8 dB with a mean of -14.4 dB. This difference is due to the SA circuits having multiple outlets whereas an individual circuit has only one outlet. The effect of

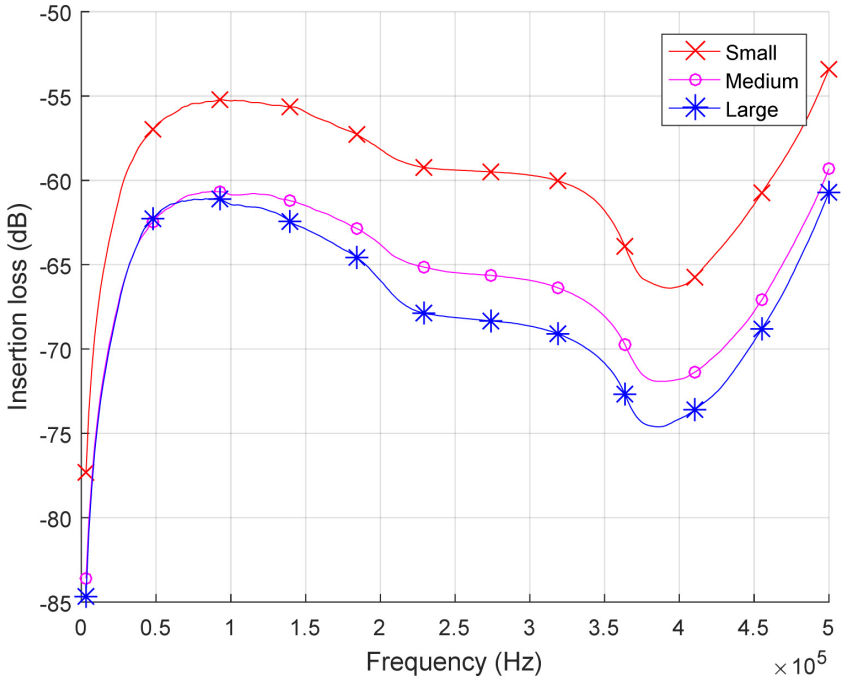

Figure 3.2: The average IL of the channels in the 1000 topologies for each house size.

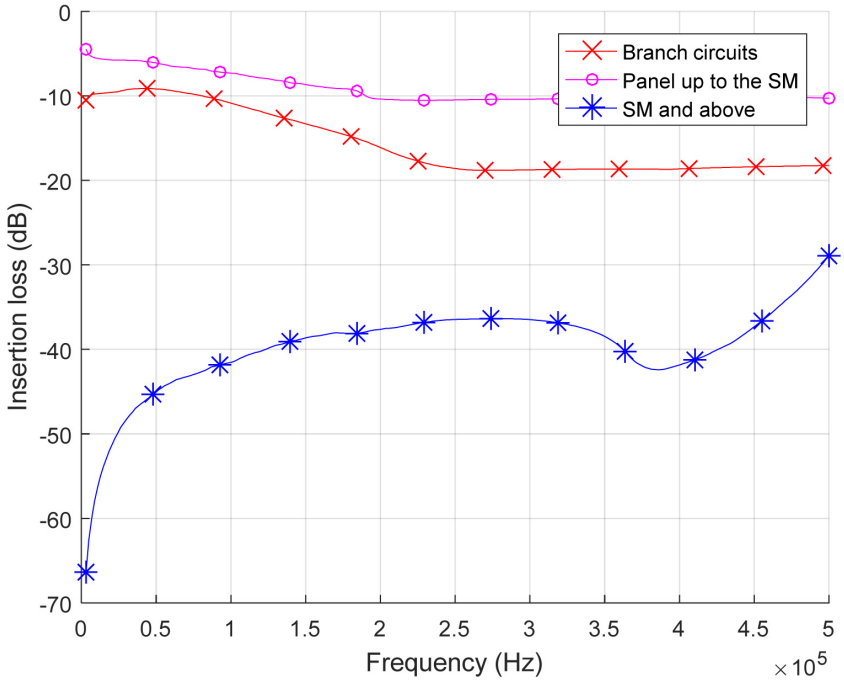

Figure 3.3: Average IL of the three parts of the home topology.

Table 3.3: Average IL of the Three Parts of the Home Topology

Part	Minimum (dB)	Maximum (dB)	Mean (dB)
Branch circuits	-18.8	-9.1	-15.68
Panel up to the SM	-10.5	-4.5	-9.21
SM and above	-66.2	-27.9	-39.67

normal and advanced circuit breakers is now examined. The average IL using only normal breakers and using AFCI and GFCI breakers as recommended by NEC [35] is shown in Figure 3.5. The difference is between -7.7 dB and -2.7 dB with a mean of -5.9 dB. This is principally because the advanced breakers have additional neutral conductors used for detecting fault currents that influence the IL.

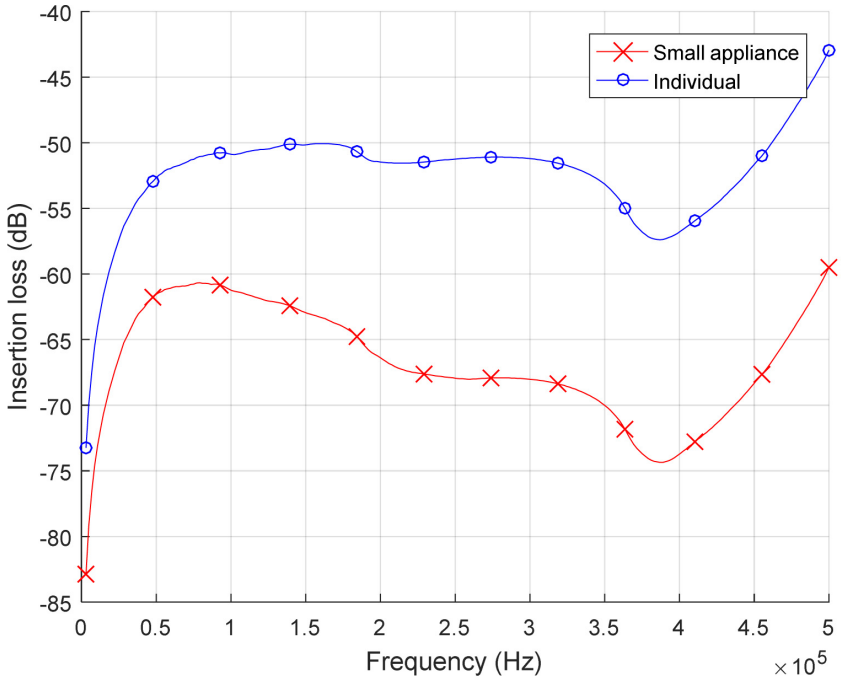

Figure 3.4: The average IL of the 9000 individual circuit channels and the 8000 SA circuit channels in the 1000 topologies.

3.3 Comparison of Channel Models

The Cañete wiring topology is a simple topology with 3 appliances as shown in Figure 3.6a [25]. This was modeled using the ABCD matrix method in [50]. The values of A, B, C and D for a conductor can be obtained from the p.u.l. R, L, G and C parameters,

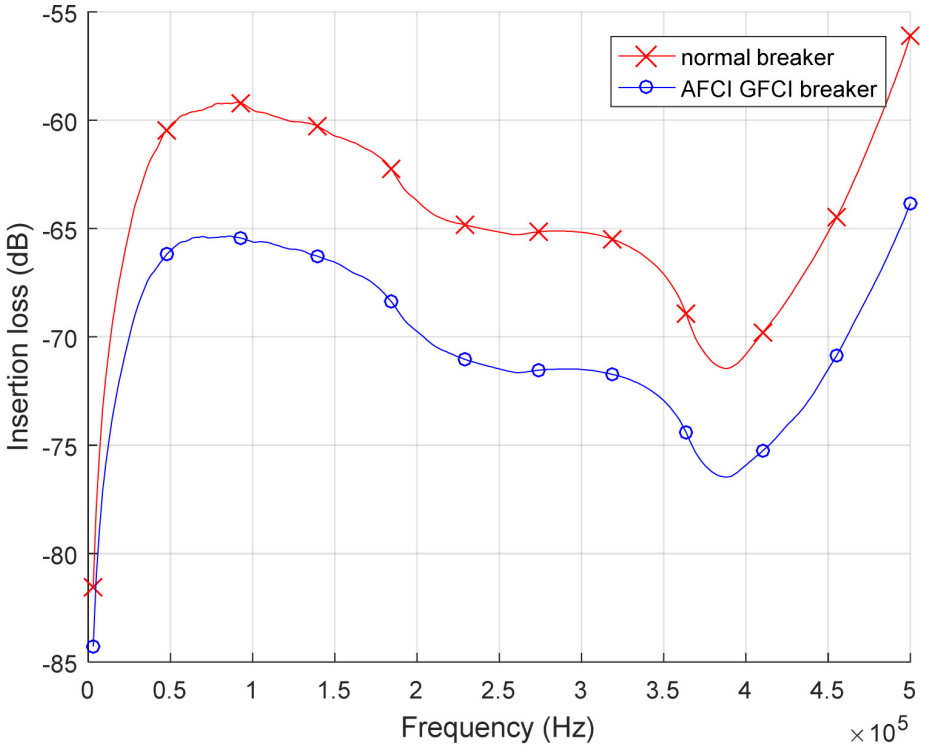

Figure 3.5: The average IL with normal breakers and AFCI and GFCI breakers.

frequency f and length l. The parameters of appliance i, $i = 1, 2, 3$, are given in Table 3.4 and the corresponding impedances $|Z_i|$ are shown in Figure 3.7.

Table 3.4: Parameters for Three Appliances

Appliance	Parameters		
	Power P_r (VA)	Resonant frequency f_0 (kHz)	Quality factor (Q_f)
1. Stereo	243.0	161.3	9.0
2. Laptop	248.8	30.3	17.4
3. TV	261.1	175.4	5.6

At junction J_i, the output impedance of conductor L_i is given by

$$Z_{outi} = \frac{A_i Z_i + B_i}{C_i Z_i + D_i} \tag{3.2}$$

so the ABCD matrix of the topology between the source Z_S and load Z_L is

$$\begin{bmatrix} A & B \\ C & D \end{bmatrix} = \begin{bmatrix} A_{(3,S)} & B_{(3,S)} \\ C_{(3,S)} & D_{(3,S)} \end{bmatrix} \begin{bmatrix} 1 & 0 \\ 1/Z_{out3} & 1 \end{bmatrix} \begin{bmatrix} A_{(2,3)} & B_{(2,3)} \\ C_{(2,3)} & D_{(2,3)} \end{bmatrix} \begin{bmatrix} 1 & 0 \\ 1/Z_{out2} & 1 \end{bmatrix} \begin{bmatrix} A_{(1,2)} & B_{(1,2)} \\ C_{(1,2)} & D_{(1,2)} \end{bmatrix} \begin{bmatrix} 1 & 0 \\ 1/Z_{out1} & 1 \end{bmatrix} \begin{bmatrix} A_L & B_L \\ C_L & D_L \end{bmatrix}. \tag{3.3}$$

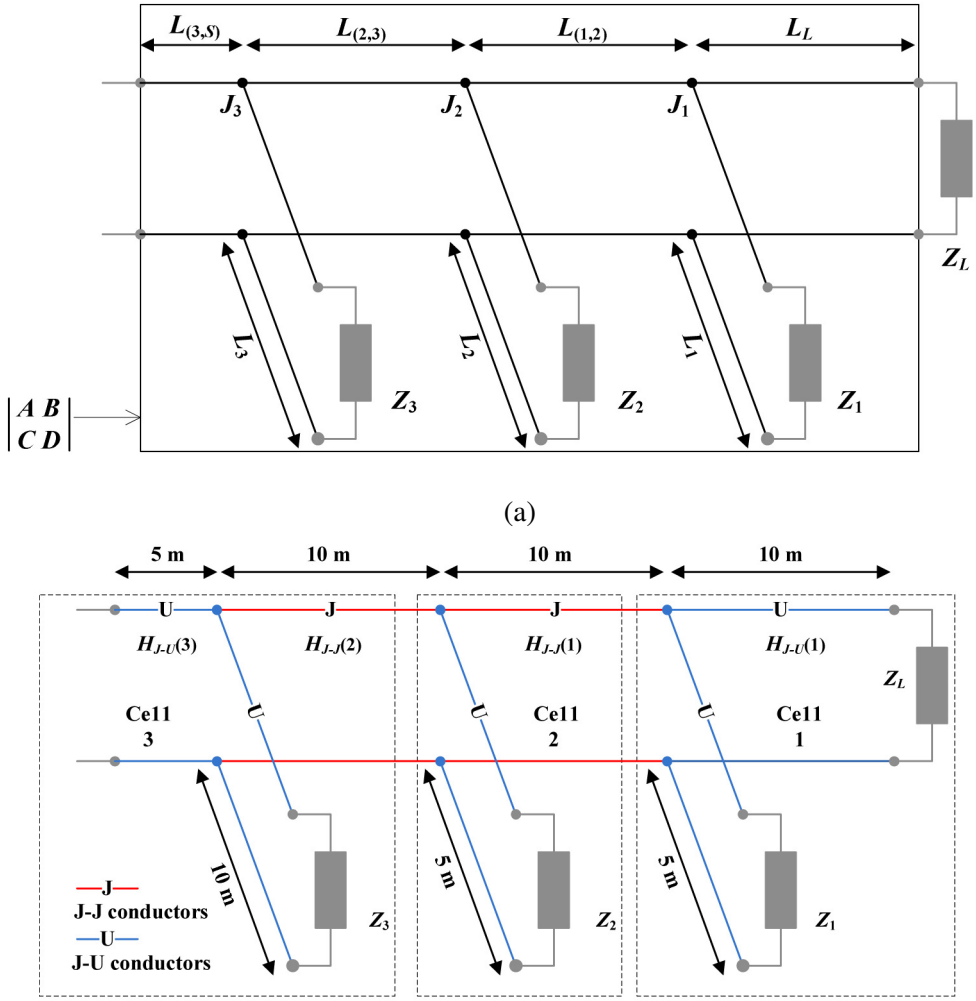

Figure 3.6: The Cañete wiring topology modeled using (a) the ABCD matrix method, and (b) the cell division method.

This can be used to obtain the transfer function H_T. Without considering Z_S [24]

$$H_T = \frac{Z_L}{AZ_L + B} \tag{3.4}$$

With the proposed method, there are three cells in the topology given in Figure 3.6a, as shown in Figure 3.6b. The impedance computation starts from cell 1 and proceeds to cell 3. The TFs of conductors $H_{J-U}(1)$, $H_{J-J}(1)$, $H_{J-J}(2)$, $H_{J-U}(3)$ were obtained and are shown in Figure 3.8. Using (2.21), the product of these TFs H_b is obtained, which provides

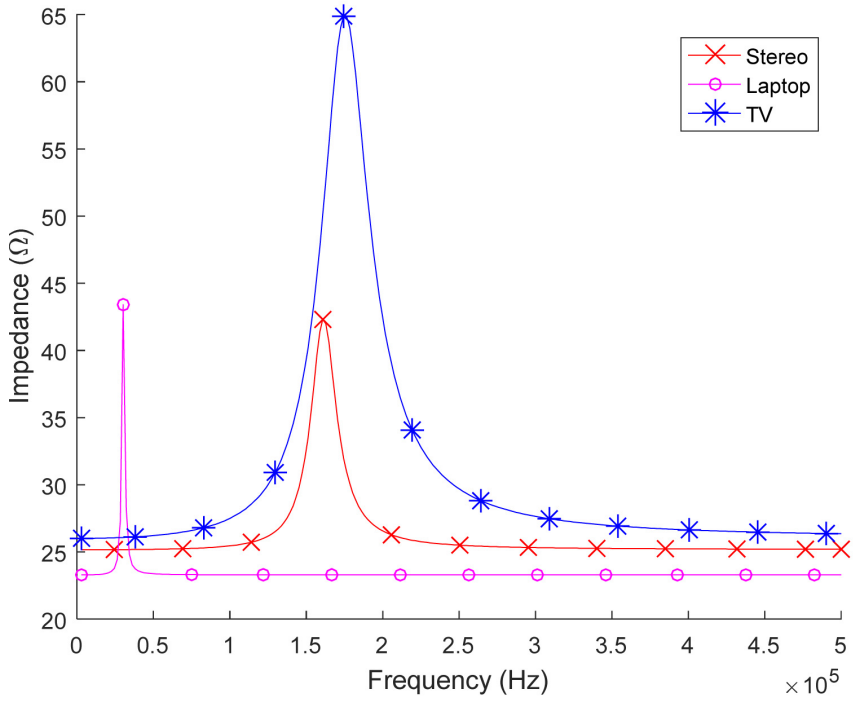

Figure 3.7: The impedances of the three appliances.

the same IL as H_T obtained from (3.4) as shown in Figure 3.9. On the other hand, the proposed method is flexible in modeling complex topologies, whereas the ABCD matrix method is not an efficient means for real applications as it uses one matrix to represent the entire topology which is impractical.

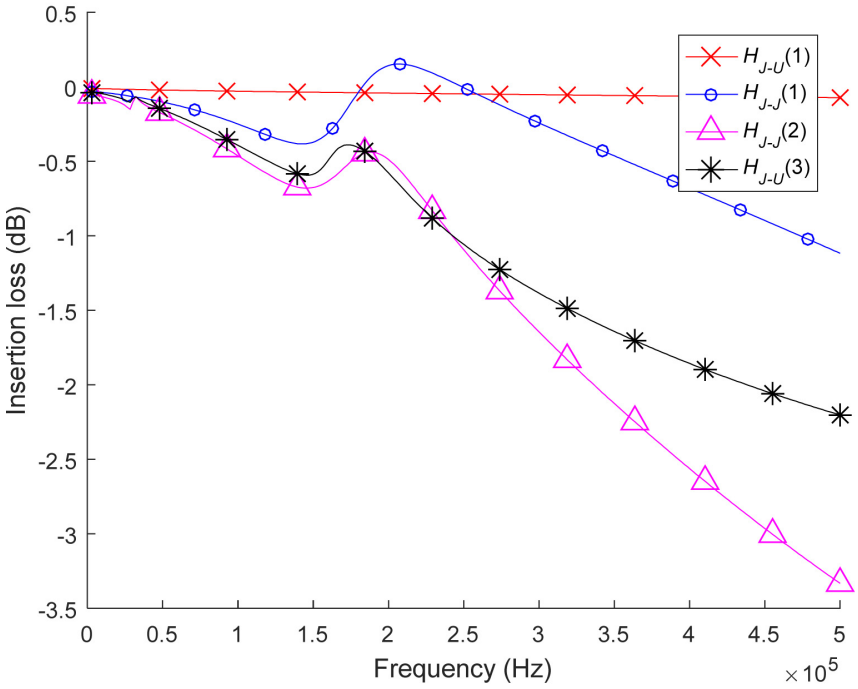

Figure 3.8: The TFs of four conductors.

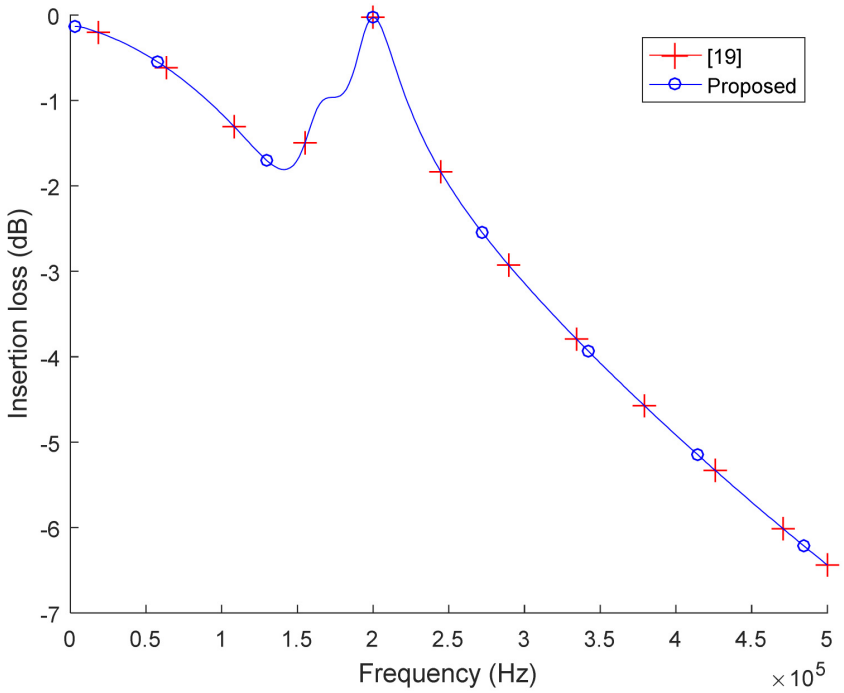

Figure 3.9: The TFs obtained using the ABCD and cell division methods.

Chapter 4

Noise Characterization

A widely accepted power line noise model characterization was given in [51], in which the noise is classified into 5 groups as shown in Figure 4.1. This indicates that the noise is complex and cannot be described as just AWGN. These 5 groups can be further categorized as background noise or impulse noise. The root mean square (RMS) amplitude of the narrowband interference and colored noise varies slowly over time, so they are called background noise [27, 52]. Narrowband interference comprises mostly modulated sinusoidal signals caused by ingress of signals from broadcast stations. Colored noise is mainly the sum of numerous noise sources with low power [53]. For instance, colored noise can be generated by a TV receiver power supply, or a malfunctioning demodulator within the TV. Electrical ballasts within home appliances such as fluorescent lamps also create colored noise. The impulse noise includes 3 groups, namely periodic impulse noise which is synchronous or asynchronous to the voltage frequency, and asynchronous impulse noise which is not periodic. Periodic impulse noise asynchronous with the voltage is mostly generated by switched-mode power supplies (SMPSs). Periodic impulse noise synchronous with the voltage is mainly caused by switching of silicon rectifier diodes with short duration (ms) and has a PSD decreasing with frequency. Asynchronous impulsive noise is caused by switching transients or the connection and disconnection of home appliances [30], both of which have a short duration (ms).

The impulse noise can be modeled as in Figure 4.2. The impulse noise sources and the receiver are located in different places in the topology. Within the frequency range 3 to 500 kHz, the dominant noise is background noise and periodic impulse noise asynchronous with the voltage [28, 54]. This chapter aims at modeling the latter which requires the channel model obtained from the topology.

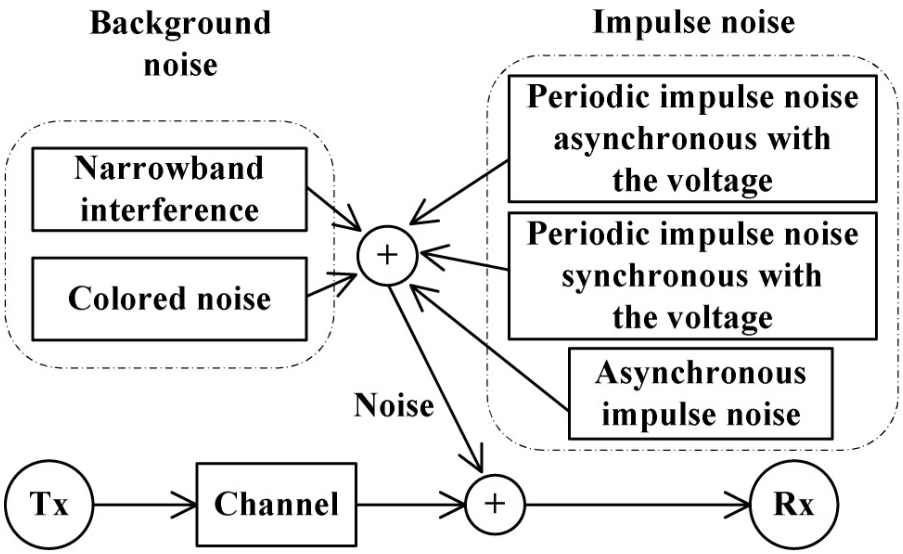

Figure 4.1: The classification of PLC noise [51].

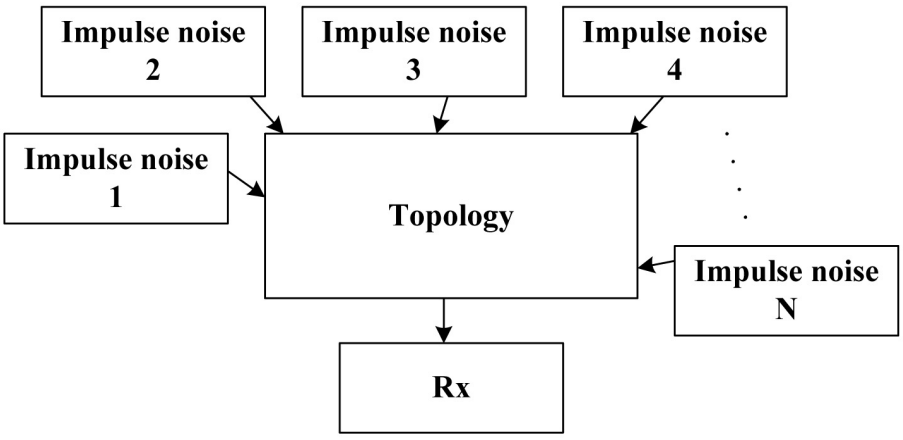

Figure 4.2: Impulse noise characterization.

In [27], A noise model was proposed which can be expressed as

$$S_{sm} = S_{bk}(f) + \sum_{i=1}^{N} [S_i(f) \times |H_i(f)|^2] \quad \text{dBm/Hz} \tag{4.1}$$

where $S_{bk}(f)$ denotes the background noise, and $S_i(f)$ and $H_i(f)$ are the impulse noise at the ith source and the transfer function of the channel between the ith source and receiver, respectively. Each source contributes to the noise PSD at the receiver and there are N sources. According to [28], 95 of 100 measured appliances are driven by SMPSs, which are the main impulse noise sources.

4.1 Noise Modeling Examples

The modeling of background and impulse noise is now considered.

4.1.1 Background Noise

The background noise can be modeled in the time domain or frequency domain. A typical time domain model for background noise was given in [27]. The background noise in the frequency domain is given by [17]

$$S_{bk} = a + b|f|^c \quad \text{dBm/Hz} \tag{4.2}$$

where a, b and c are as follows [54]. The parameter a has a truncated normal distribution within three intervals as in Table 4.1. This table includes the mean, standard deviation (std) and probability of a in each interval. The parameter b has a lognormal distribution with mean 12.95 and standard deviation 4.42 while c has a normal distribution with mean -0.94 and std 0.49.

Table 4.1: Distribution of a

	Mean	Standard deviation (std)	Probability
$-120 \leq a < 0$	105.07	4.70	0.66
$-200 \leq a < -120$	142.71	21.51	0.29
$a < -200$	656.41	619.16	0.05

The frequency f is between 3 kHz and 500 kHz. Within these frequencies, S_{bk} has a best case noise floor of -130 dBm/Hz, i.e. S_{bk} is between 0 and -130 dBm/Hz with a

minimum close to -130 dBm/Hz, and a worst case of -145 dBm/Hz [55]. In [31], [32] and [34], background noise models similar to that in [54] were proposed for the CENELENC A band (10 kHz to 95 kHz), and thus cannot be used for the frequency band between 3 kHz and 500 kHz. Background noise was generated 1000 times in MATLAB using (4.2) and the parameters above. The curves representing the best and worst cases are shown in Figure 4.3. The parameters a, b, and c are (-146.9608, 589.2164, -0.3881) in the best case and (-129.5523, 1.4002×10^4, -0.9301) in the worst case, respectively.

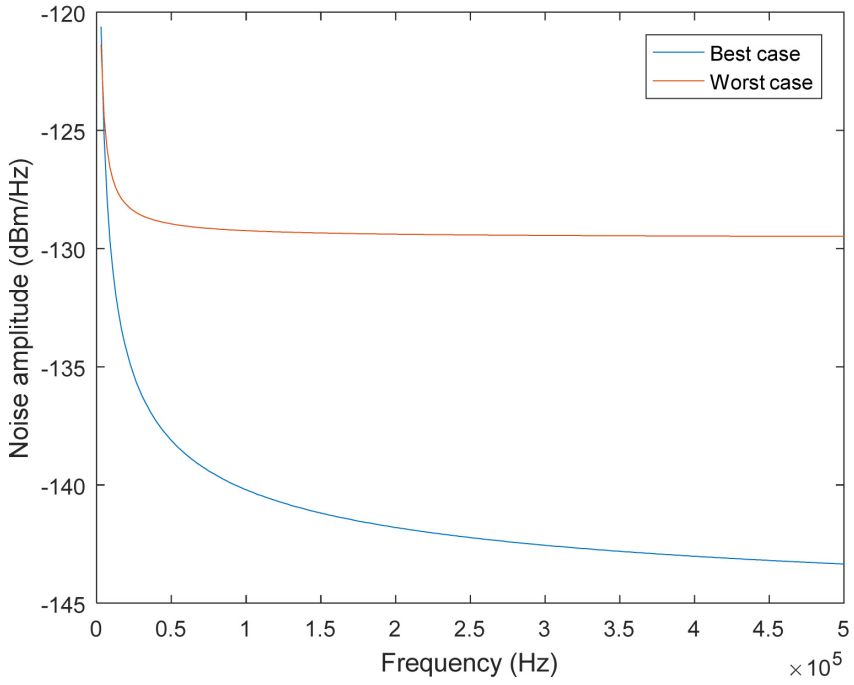

Figure 4.3: The best and worst cases of background noise.

4.1.2 Impulse Noise

A low voltage indoor power line noise model for impulse noise at the receiver was given in [54]

$$S_N(f) = \sum_{i=1}^{N} a_i \exp\left(-\frac{(f-f_i)^2}{2\sigma_i^2}\right) \quad \text{dBm/Hz} \tag{4.3}$$

where N is the number of impulse sources. a_i is the amplitude of the impulse noise at the receiver, which follows a Gamma probability density function (PDF)

$$f(x;\alpha,\beta) = \frac{1}{\beta^{\alpha}\Gamma(\alpha)} x^{\alpha-1} e^{\frac{-x}{\beta}} \tag{4.4}$$

where

$$\Gamma(\alpha) = \int_0^\infty t^{\alpha-1} e^{-t} dt \tag{4.5}$$

is a Gamma function with $\alpha = 2.79$ the shape parameter and $\beta = 5.34$ is the scale parameter. f_i is the center frequency of the ith impulse signal, which has a truncated normal distribution within five frequency intervals as given in Table 4.2. This table includes the mean, standard deviation and probability of f_i within each interval.

Table 4.2: Distribution of f_i

Range (kHz)	Mean (kHz)	σ_i (kHz)	Probability
$3 \leq f_i \leq 100$	55.90	22.11	0.27
$100 < f_i \leq 200$	144.00	24.89	0.20
$200 < f_i \leq 300$	258.61	29.75	0.21
$300 < f_i \leq 400$	346.74	26.81	0.18
$400 < f_i \leq 500$	453.15	30.18	0.14

In this chapter, the impulse noise at the Rx is obtained from [27] as

$$S_{sm} = \sum_{i=1}^{N} [S_i \times |H_i|^2] \quad \text{dBm/Hz} \tag{4.6}$$

where S_i is the impulse noise at the ith source which is given by

$$S_i = A_i \exp\left(-\frac{(f - f_i)^2}{2\sigma_i^2}\right) \tag{4.7}$$

where the amplitude A_i is obtained using

$$A_i = \frac{|U_i|^2}{|R_i|} \tag{4.8}$$

where U_i is the voltage of impulse noise at the source given in Table 4.3 [56] and R_i is the load impedance.

Table 4.3: Impulse Noise Parameters

Mean (V)	Std (V)	Min (V)	Max (V)
0.0301	0.0133	0.0141	0.0495

The models (4.3) and (4.6) are now compared. A medium size house is now considered and the appliances in the topology are as follows. The 9 individual circuits include 9 plugs

in outlets. The 4 BSL SA circuits have 40 outlets and half are open. The 2 kitchen SA circuits have 20 outlets and half are open. The laundry SA circuit has 4 outlets and half are open. The bathroom SA circuit has 4 outlets and half are open. The 5 lighting circuits include 40 lights. Thus there are approximately $9 + (40 + 20 + 4 + 4) \times 0.5 + 40 = 83$ appliances in the topology. A random medium size home topology is now obtained with 43 appliances turned on. Thus there are $N = 43$ impulse noise sources. For each source, f_i and σ_i are obtained using Table 4.2. For the impulse noise model (4.3), the amplitude a_i of each source is obtained using (4.4). For the proposed impulse noise model (4.6), the amplitudes A_i are obtained using the truncated Gaussian distribution given in Table 4.3 and the transfer functions between the 43 appliances and smart meter are obtained from the home topology. Two noise models are obtained using (4.1) with the corresponding PSDs given in Figure 4.4a and cumulative distribution functions (CDFs) in Figure 4.4b. Altogether 27 impulse noise peaks are observed (less than 43), indicating that some peaks with close center frequencies merged. The PSD differences between the two noise models at these peaks are given in Table 4.4 where the minimum is 0.76 dBm/Hz at 170.62 kHz, and the maximum is 20.92 dBm/Hz at 180.36 kHz.

Table 4.4: Power Spectral Density Differences Between (4.3) and (4.6) at the Impulse Noise Peaks

f (kHz)	20.54	40.03	59.52	75.11	82.91	86.81	104.35
PSD (dBm/Hz)	9.14	2.17	11.20	3.59	8.63	7.24	2.57
f (kHz)	110.20	121.89	170.62	180.36	199.85	213.49	236.88
PSD (dBm/Hz)	6.19	10.47	0.76	20.92	1.51	6.86	4.10
f (kHz)	248.58	256.37	260.27	293.40	310.95	314.84	334.33
PSD (dBm/Hz)	4.41	7.22	5.99	1.77	4.97	4.01	12.92
f (kHz)	355.77	367.47	379.16	441.53	461.02	468.82	
PSD (dBm/Hz)	3.46	11.01	8.30	9.90	11.66	4.05	

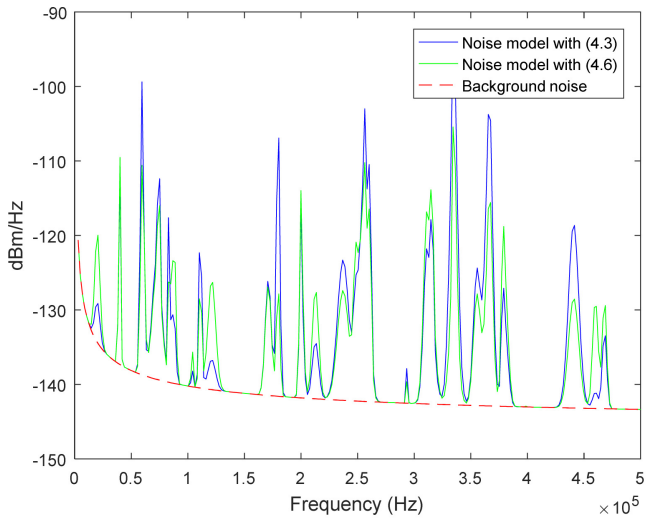

(a)

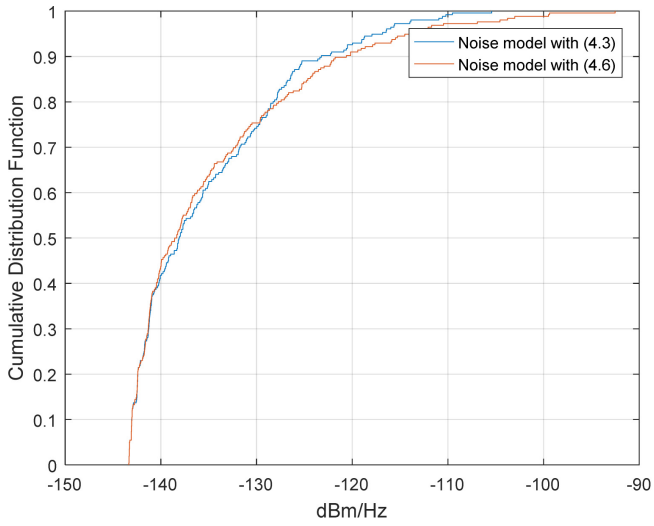

(b)

Figure 4.4: (a) The PSD of the noise at the receiver, and (b) the corresponding CDF.

Chapter 5

Conclusions

In this thesis, power line communication (PLC) channel models were developed for a home area network (HAN). The thesis started with an introduction to smart meters (SMs), including the services they provide and the standards associated with PLC. PLC based research was introduced and a literature review of PLC HAN channel modeling was given. Noise modeling was also discussed.

In Chapter 2, the wiring topology of a split-phase power system was modeled in detail. It has three parts, the topology above the SM, the electrical panel up to the SM and the branch circuits. The parameters of the components within the topology were provided. These components are conductors, appliances, modems, the smart meter and the secondary transformer. A cell division (CD) method was proposed to obtain a channel model using this topology. This approach uses the actual parameters of the topology components and thus provides an accurate model.

Chapter 3 presented results for random topologies. Three topology sizes, normal breakers and advanced breakers, the three parts of the topology, as well as individual and small appliance (SA) circuits were considered. The CD method was shown to be an efficient means of modeling HAN topologies. This method was used to develop a model for the Cañete wiring topology which is well-known in the literature. The results indicate that the CD method provides accurate channel models. This method can also be used to obtain channel models for other electrical systems such as in an electric vehicle or a solar panel, and for any building topology.

A noise model for a HAN PLC channel was developed in Chapter 4 which is comprised of background and impulse noise. The impulse noise at the receiver was obtained using the channel transfer functions (CTFs) between the impulse noise sources and the receiver, and the impulse noise at the sources. This model was compared with the literature which

shows good agreements in the PSDs and CDFs of the models. These results indicate that the proposed model is suitable for modeling noise in HANs.

The following topics are suggested for future work. The receiver side bit error rate (BER) can be obtained for performance evaluation of PLC in the HAN using the proposed models. In the physical (PHY) layer, different modulation schemes can be compared to find the most appropriate solution. In the medium access control (MAC) layer, CSMA, CSMA/CA and TDMA can be evaluated to determine which of the contention and contention-free mechanisms is appropriate for SG applications. From the perspective of noise modeling, the impulse noise generated in electrical switch and thermostat on and off events, electrical plug insertion and removal and electrical engine start events [56] were not covered in this thesis. The influence of these transient events is a promising topic for future PLC research.

Appendix A

The Inner Self Inductance of a Circular or Rectangular Conductor

The inner self inductance without considering the skin depth is given in [38]. In this appendix, the p.u.l. inner inductance with skin effect is discussed. Consider a circular conductor as shown in Figure A.1a with a skin depth greater than the radius. The magnetic flux in the circle with radius r_c is

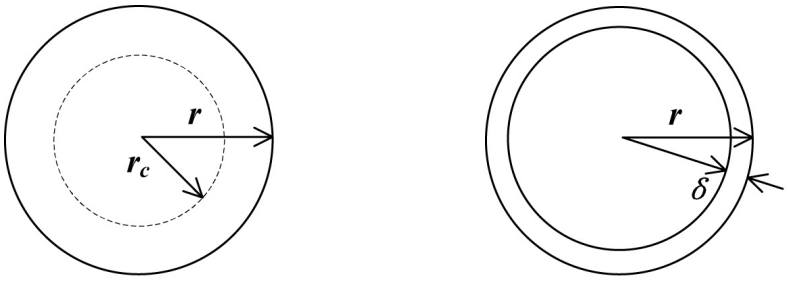

(a) (b)

Figure A.1: Circular conductors when (a) the skin depth is greater than the radius, and (b) otherwise.

$$\oint B \times \mathrm{d}l = \mu I \times \left(\frac{r_c}{r}\right)^2 \text{ where } B = \frac{\mu I r_c}{2\pi r^2}. \tag{A.1}$$

The magnetic field energy is

$$\frac{1}{2\mu}\int B^2 \times \mathrm{d}V = \frac{1}{2}LI^2 \tag{A.2}$$

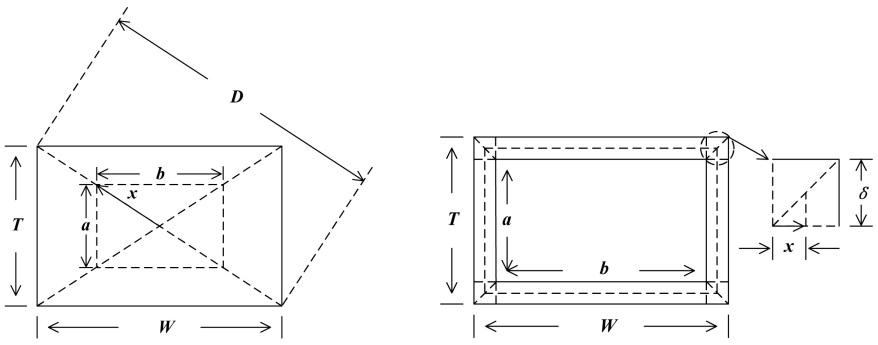

(a) (b)

Figure A.2: A rectangular conductor when (a) the skin depth is greater than half the smaller of the width W and depth T, and (b) otherwise.

where $\mathrm{d}V = r_c \mathrm{d}r_c \mathrm{d}\theta \mathrm{d}Z$. The inner self inductance is

$$L_{c,in} = \frac{\mu}{4\pi^2 r^4} \int_0^1 \mathrm{d}Z \int_0^{2\pi} \mathrm{d}\theta \int_0^r r_c^3 \mathrm{d}r_c = \frac{\mu}{8\pi}. \tag{A.3}$$

Figure A.1b shows that when the skin depth is much smaller than the radius

$$L_{c,in} = \frac{\mu}{4\pi^2 r^4} \int_0^1 \mathrm{d}Z \int_0^{2\pi} \mathrm{d}\theta \int_{r-\delta}^r r_c^3 \mathrm{d}r_c = \frac{\mu}{8\pi} \left[1 - \left(1 - \frac{\delta}{r} \right)^4 \right] \tag{A.4}$$

For a rectangular conductor with a skin depth greater than half the smaller of the width W and depth T, as shown in Figure A.2a, the current flows in the entire cross section area. The magnetic flux in the rectangle with side lengths a and b is

$$\oint B \times \mathrm{d}l = \mu I \times \frac{ab}{TW} \tag{A.5}$$

where $a = \dfrac{2xT}{D}$ and $b = \dfrac{2xW}{D}$, which gives

$$B = \frac{\mu I x}{D(T+W)} \tag{A.6}$$

in which $D = \sqrt{W^2 + T^2}$. The magnetic field energy is

$$\frac{1}{2\mu} \int B^2 \times \mathrm{d}V = \frac{1}{2} L I^2$$

where $\mathrm{d}V = 2(a+b)\mathrm{d}x$ so that

$$\frac{1}{2\mu}\int_0^{D/2}\left[\frac{\mu I x}{D(T+W)}\right]^2 \times 2\left(\frac{2xT}{D}+\frac{2xW}{D}\right)\mathrm{d}x = \frac{1}{2}LI^2 \tag{A.7}$$

so

$$L_{c,in} = \frac{\mu\sqrt{W^2+T^2}}{16(W+T)} \tag{A.8}$$

When the skin depth is less than half the smaller of the width W and depth T, as shown in Figure A.2b, the magnet flux in the rectangle with width $b+2x$ and depth $a+2x$ satisfies

$$\oint B \times \mathrm{d}l = \mu I \times \frac{2ax+2bx+4x^2}{2a\delta+2b\delta+4\delta^2} \tag{A.9}$$

where $a = T-2\delta$ and $b = W-2\delta$, which gives

$$B = \mu I \times \frac{2ax+2bx+4x^2}{2a\delta+2b\delta+4\delta^2} \times \frac{1}{2(a+b+4x)} \tag{A.10}$$

The magnetic field energy is

$$\frac{1}{2\mu}\int B^2 \times \mathrm{d}V = \frac{1}{2}LI^2$$

where $\mathrm{d}V = 2(a+b+4x)\mathrm{d}x$ so that

$$\frac{1}{2\mu}\int_0^{\delta}\left[\mu I \times \frac{2ax+2bx+4x^2}{2a\delta+2b\delta+4\delta^2} \times \frac{1}{2(a+b+4x)}\right]^2 \times 2(a+b+4x)\mathrm{d}x = \frac{1}{2}LI^2 \tag{A.11}$$

$$\begin{aligned} L =& \frac{\mu}{(2a\delta+2b\delta+4\delta^2)^2}\left[\frac{1}{2}x^4+\frac{1}{2}(a+b)x^3-\frac{1}{16}(a+b)^2x^2\right. \\ &\left.+\frac{1}{32}(a+b)^3x-\frac{1}{128}(a+b)^4\ln(a+b+4x)\right]_0^{\delta} \end{aligned} \tag{A.12}$$

Then the inner inductance is

$$\begin{aligned} L_{r,in} =& \frac{\mu}{2\delta^2(W+T-2\delta)^2}\left[\frac{\delta^4}{4}+\frac{\delta^3}{4}(W+T-4\delta)-\frac{\delta^2}{32}(W+T-4\delta)^2\right. \\ &\left.+\frac{\delta}{64}(W+T-4\delta)^3-\frac{(W+T-4\delta)^4}{256}\ln\left(\frac{W+T}{W+T-4\delta}\right)\right]. \end{aligned} \tag{A.13}$$

Bibliography

[1] O. Fitzgerald and B. Ugochukwu, *Implementing the Paris Agreement: The Relevance of Human Rights to Climate Action*. Centre for International Governance Innovation, CA, 2016.

[2] S. Galli, A. Scaglione, and Z. Wang, "For the grid and through the grid: The role of power line communications in the smart grid," *Proceedings of the IEEE*, vol. 99, no. 6, pp. 998–1027, 2011.

[3] B. Adebisi, A. Khalid, Y. Tsado, and B. Honary, "Narrowband PLC channel modelling for smart grid applications," *Proc. International Symposium on Communication Systems, Networks Digital Sign*, 2014, pp. 67–72.

[4] B. Adebisi, A. Treytl, and A. Haidine, "IP-centric high rate narrowband PLC for smart grid applications," *IEEE Communications Magazine*, vol. 49, no. 12, pp. 46–54, 2011.

[5] A. Haidine, B. Adebisi, A. Treytl, and H. Pille, "High speed narrowband PLC in smart grid landscape state of the art," *Proc. IEEE International Symposium on Power Line Communications and its Applications*, 2011, pp. 468–473.

[6] Q. Yu and R. J. Johnson, "Smart grid communications equipment: EMI, safety, and environmental compliance testing considerations," *Bell Labs Technical Journal*, vol. 16, no. 3, pp. 109–131, 2011.

[7] S. Yussof, M. E. Rusli, Y. Yusoff, R. Ismail, and A. A. Ghapar, "Financial impacts of smart meter security and privacy breach," *Proc. International Conference on Information Technology and Multimedia*, 2014, pp. 11–14.

[8] J. Domínguez, J. P. Chaves-Ávila, T. G. S. Román, and C. Mateo, "The economic impact of demand response on distribution network planning," *Proc. Power Systems Computation Conference*, 2016, pp. 1–7.

[9] A. Pasdar and S. Mirzakuchaki, "A solution to remote detecting of illegal electricity usage based on smart metering," *Proc. International Workshop on Soft Computing Applications*, 2007, pp. 163–167.

[10] IEEE standard for broadband over power line networks: Medium access control and physical layer specifications, *IEEE Std 1901-2010*, pp. 1–15, 2010.

[11] IEEE standard for low-frequency (less than 500 kHz) narrowband power line communications for smart grid applications, *IEEE Std 1901.2-2013*, pp. 1–35, 2013.

[12] K. Sharma and L. M. Saini, "Power line communications for smart grid: Progress, challenges, opportunities and status," *Renewable and Sustainable Energy Reviews*, vol. 67, no. 1, pp. 704–751, 2017.

[13] S. Panchadcharam, G. A. Taylor, I. Pisica, and M. R. Irving, "Modeling and analysis of noise in power line communication for smart metering," *Proc. IEEE Power and Energy Society General Meeting*, 2012, pp. 1–8.

[14] M. A. Sonmez, M. A. Zehir, M. Bagriyanik, and O. Nak, "Impulsive noise survey on power line communication networks up to 125 kHz for smart metering infrastructure in systems with solar inverters in Turkey," *Proc. Renewable Energy Research and Applications*, 2013, pp. 705–710.

[15] O. Neagu and W. Hamouda, "Performance of smart grid communication in the presence of impulsive noise," *Proc. International Conference on Selected Topics in Mobile Wireless Networking*, 2016, pp. 1–5.

[16] Z. Zhang, Z. Qin, L. Zhu, J. Weng, and K. Ren, "Cost-friendly differential privacy for smart meters: Exploiting the dual roles of the noise," *IEEE Transactions on Smart Grid*, vol. 8, no. 2, pp. 619–626, 2016.

[17] T. Esmailian, F. R. Kschischang, and P. G. Gulak, "In-building power lines as high-speed communication channels: Channel characterization and a test channel ensemble," *International Journal of Communication Systems*, vol. 16, no. 5, pp. 381–400, 2003.

[18] S. Galli and T. Banwell, "A deterministic frequency-domain model for the indoor power line transfer function," *IEEE Journal on Selected Areas in Communications*, vol. 24, no. 7, pp. 1304–1316, 2006.

[19] T. Banwell and S. Galli, "A novel approach to the modeling of the indoor power line channel part I: Circuit analysis and companion model," *IEEE Transactions on Power Delivery*, vol. 20, no. 2, pp. 655–663, 2005.

[20] S. Galli and T. Banwell, "A novel approach to the modeling of the indoor power line channel part II: Transfer function and its properties," *IEEE Transactions on Power Delivery*, vol. 20, no. 3, pp. 1869–1878, 2005.

[21] G. Marrocco, D. Statovci, and S. Trautmann, "A PLC broadband channel simulator for indoor communications," *Proc. IEEE International Symposium on Power Line Communications and its Applications*, 2013, pp. 321–326.

[22] R. Nizigiyimana, J. C. Lebunetel, Y. Raingeaud, A. Achouri, P. Ravier, and G. Lamarque, "Characterization and modeling breakers effect on power line communications," *Proc. IEEE International Symposium on Power Line Communications and its Applications*, 2014, pp. 36–41.

[23] A. M. Tonello and F. Versolatto, "Bottom-up statistical PLC channel modeling-part I: Random topology model and efficient transfer function computation," *IEEE Transactions on Power Delivery*, vol. 26, no. 2, pp. 891–898, 2011.

[24] F. Aalamifar, A. Schlogl, D. Harris, and L. Lampe, "Modelling power line communication using network simulator-3," *Proc. IEEE Global Communications Conference*, 2013, pp. 2969–2974.

[25] F. J. Cañete, J. A. Cortés, L. Díez, and J. T. Entrambasaguas, "A channel model proposal for indoor power line communications," *IEEE Communications Magazine*, vol. 49, no. 12, pp. 166–174, 2011.

[26] T. Guzel, E. Ustunel, H. B. Celebi, H. Delic, and K. Mihcak, "Noise modeling and OFDM receiver design in power-line communication," *IEEE Transactions on Power Delivery*, vol. 26, no. 4, pp. 2735–2742, 2011.

[27] H. Meng, Y. L. Guan, and S. Chen, "Modeling and analysis of noise effects on broadband power-line communications," *IEEE Transactions on Power Delivery*, vol. 20, no. 2, pp. 630–637, 2005.

[28] D. Chariag, D. Guezgouz, J. C. Le Bunetel, and Y. Raingeaud, "Modeling and simulation of temporal variation of channel and noise in indoor power-line network," *IEEE Transactions on Power Delivery*, vol. 27, no. 4, pp. 1800–1808, 2012.

[29] J. A. Cortes, L. Diez, F. J. Canete, and J. Lopez, "Analysis of the periodic impulsive noise asynchronous with the mains in indoor PLC channels," *Proc. IEEE International Symposium on Power Line Communications and its Applications*, 2009, pp. 26–30.

[30] J. A. Cortes, L. Diez, F. J. Canete, and J. J. Sanchez-Martinez, "Analysis of the indoor broadband power-line noise scenario," *IEEE Transactions on Electromagnetic Compatibility*, vol. 52, no. 4, pp. 849–858, 2010.

[31] Z. Gu, H. L. Liu, and D. W. Liu, "Modeling the noise in narrowband power line communication," *International Journal of Control and Automation, Science and Engineering Research Support Society*, vol. 9, no. 2, pp. 41–48, 2016.

[32] M. Katayama, T. Yamazato, and H. Okada, "A mathematical model of noise in narrowband power line communication systems," *IEEE Journal on Selected Areas in Communications*, vol. 24, no. 7, pp. 1267–1276, 2006.

[33] M. Nassar, A. Dabak, and I. H. Kim, "Cyclostationary noise modeling in narrowband powerline communication for smart grid applications," *Proc. IEEE International Conference on Acoustics, Speech and Signal Processing*, 2012, pp. 3089–3092.

[34] O. Ohno, M. Katayama, and T. Yamazato, "A simple model of cyclostationary powerline noise for communication systems," *Proc. IEEE International Symposium on Power Line Communications and its Applications*, 2005, pp. 115–122.

[35] M. W. Earley, *National Electrical Code*. NFPA 70, USA, 2013.

[36] Schneider Electric, "HomeLine Loadcentres and Circuit Breakers Selection Guide," https://www.schneider-electric.ca/documents/electrical-distribution/en/shared/catalogue/DE1.pdf.

[37] D. J. Hepler, P. R. Wallach, and D. Hepler, *Drafting and Design for Architecture & Construction*. Cengage Learning, USA, 2012.

[38] E. B. Rosa, "The self and mutual inductances of linear conductors," *Bulletin of the Bureau of Standards*, vol. 4, no. 2, pp. 301–344, 1907.

[39] C. Hoer and C. Love, "Exact inductance equations for rectangular conductors with applications to more complicated geometries," *Journal of Research of the National Bureau of Standards*, vol. 69, no. 2, pp. 127–137, 1965.

[40] F. Versolatto and A. M. Tonello, "An MTL theory approach for the simulation of MIMO power-line communication channels," *IEEE Transactions on Power Delivery*, vol. 26, no. 3, pp. 1710–1717, 2011.

[41] J. Dickinson and P. J. Nicholson, "Calculating the high frequency transmission line parameters of power cables," *Proc. IEEE International Symposium on Power Line Communications and its Applications*, 1997, pp. 127–133.

[42] C. Miller, *Illustrated Guide to the NEC*. Nelson Education, USA, 2014.

[43] I. H. Cavdar and K. Engin, "Measurements of impedance and attenuation at CENELEC bands for power line communications systems," *Sensors*, vol. 8, no. 12, pp. 8027–8036, 2008.

[44] B. Sudiarto, A. N. Widyanto, and H. Hirsch, "Equivalent circuit identification of standby mode operation for some household appliances in frequency range 9-150 kHz for the investigation of conducted disturbance in low voltage installations," *Proc. International Symposium on Electromagnetic Compatibility*, 2016, pp. 835–838.

[45] R. M. Vines, H. J. Trussell, K. C. Shuey, and J. B. O'Neal, "Impedance of the residential power-distribution circuit," *IEEE Transactions on Electromagnetic Compatibility*, vol. 27, no. 1, pp. 6–12, 1985.

[46] "Ohm's law and temperature resistance charts," *Students' Quarterly Journal*, vol. 3, no. 9, pp. 46–55, 1932.

[47] J. M. H. Duffy and B. Thomas, "Frequency-selective circuit protection arrangements," US Patent 6,437,955, 2002.

[48] J. P. Wilkinson, "Nonlinear resonant circuit devices," US Patent 3,624,125, 1990.

[49] B. B. Neiger, "Arc fault detector with circuit interrupter," US Patent 6,088,205, 2000.

[50] T. C. Banwell and S. Galli, "On the symmetry of the power line channel," *Proc. IEEE International Symposium on Power Line Communications and its Applications*, 2001, pp. 325–330.

[51] M. Zimmermann and K. Dostert, "Analysis and modeling of impulsive noise in broadband powerline communications," *IEEE Transactions on Electromagnetic Compatibility*, vol. 44, no. 1, pp. 249–258, 2002.

[52] M. Gotz, M. Rapp, and K. Dostert, "Power line channel characteristics and their effect on communication system design," *IEEE Communications Magazine*, vol. 42, no. 4, pp. 78–86, 2004.

[53] G. Lpez, J. I. Moreno, E. Snchez, and C. Martinez, "Noise sources, effects and countermeasures in narrowband power-line communications networks: A practical approach," *Energies*, vol. 10, no. 8, pp. 1–41, 2017.

[54] H. Gassara, F. Rouissi, and A. Ghazel, "Narrowband stationary noise characterization and modelling for power line communication," *Proc. International Symposium on Communications and Information Technologies*, 2013, pp. 148–153.

[55] W. Y. Chen, *Home Networking Basis: Transmission Environments and Wired/Wireless Protocols*. Prentice Hall, USA, 2003.

[56] M. Tlich, H. Chaouche, A. Zeddam, and F. Gauthier, "Impulsive noise characterization at source," *Proc. IFIP Wireless Days*, 2008, pp. 1–6.